PLOS PATHOGENS

RESEARCH ARTICLE

Spike substitution T813S increases Sarbecovirus fusogenicity by enhancing the usage of TMPRSS2

Yong Ma[1☯], Pengbin Li[1☯], Yunqi Hu[1☯], Tianyi Qiu[2], Lixiang Wang[3], Hongjie Lu[1], Kexin Lv[1], Mengxin Xu[1], Jiaxin Zhuang[4], Xue Liu[4], Suhua He[5], Bing He[1], Shuning Liu[1], Lin Liu[1], Yuanyuan Wang[1], Xinyu Yue[1], Yanmei Zhai[1], Wanyu Luo[1], Haoting Mai[1], Yu Kuang[1], Shifeng Chen[6], Feng Ye[6], Na Zhou[6], Wenjing Zhao[4], Jun Chen[3], Shoudeng Chen[5], Xiaoli Xiong[7], Mang Shi[4], Ji-An Pan[4]*, Yao-Qing Chen[1,8]*

1 School of Public Health (Shenzhen), Shenzhen Campus of Sun Yat-sen University, Shenzhen, China, **2** Institute of Clinical Science, Zhongshan Hospital, Shanghai Medical College, Fudan University, Shanghai, China, **3** Department of Immunology and Microbiology, Zhongshan School of Medicine, Sun Yat-sen University, Guangzhou, China, **4** The Center for Infection and Immunity Study and Molecular Cancer Research Center, School of Medicine, Shenzhen Campus of Sun Yat-sen University, Shenzhen, China, **5** Molecular Imaging Center, Guangdong Provincial Key Laboratory of Biomedical Imaging, the Fifth Affiliated Hospital, Sun Yat-sen University, Zhuhai, China, **6** The 74(th) Group Army Hospital, Guangzhou, China, **7** State Key Laboratory of Respiratory Disease, CAS Key Laboratory of Regenerative Biology, Guangdong Provincial Key Laboratory of Stem Cell and Regenerative Medicine, Guangzhou Institutes of Biomedicine and Health, Chinese Academy of Sciences, Guangzhou, China, **8** National Medical Products Administration Key Laboratory for Quality Monitoring and Evaluation of Vaccines and Biological Products, Sun Yat-sen University, Guanzhou, China

☯ These authors contributed equally to this work.
* panjan@mail.sysu.edu.cn (JAP); chenyaoqing@mail.sysu.edu.cn (YQC)

OPEN ACCESS

Citation: Ma Y, Li P, Hu Y, Qiu T, Wang L, Lu H, et al. (2023) Spike substitution T813S increases Sarbecovirus fusogenicity by enhancing the usage of TMPRSS2. PLoS Pathog 19(5): e1011123. https://doi.org/10.1371/journal.ppat.1011123

Editor: Jacob S. Yount, The Ohio State University, UNITED STATES

Received: January 14, 2023

Accepted: April 24, 2023

Published: May 17, 2023

Data Availability Statement: All relevant data are within the manuscript and its Supporting Information files.

Funding: This project was funded by the National Key R&D Program of China (grant number: 2022YFC2304204 to YQC); the National Natural Science Foundation of China (32000648 to YM); the National Natural Science Foundation of China (NO. 92169104, 31970881, 82150204,32171192, 31971161 and 31900546); Shenzhen Science and Technology Program (Grant No. RCJC20210706092009004,

Abstract

SARS-CoV Spike (S) protein shares considerable homology with SARS-CoV-2 S, especially in the conserved S2 subunit (S2). S protein mediates coronavirus receptor binding and membrane fusion, and the latter activity can greatly influence coronavirus infection. We observed that SARS-CoV S is less effective in inducing membrane fusion compared with SARS-CoV-2 S. We identify that S813T mutation is sufficient in S2 interfering with the cleavage of SARS-CoV-2 S by TMPRSS2, reducing spike fusogenicity and pseudoparticle entry. Conversely, the mutation of T813S in SARS-CoV S increased fusion ability and viral replication. Our data suggested that residue 813 in the S was critical for the proteolytic activation, and the change from threonine to serine at 813 position might be an evolutionary feature adopted by SARS-2-related viruses. This finding deepened the understanding of Spike fusogenicity and could provide a new perspective for exploring *Sarbecovirus*' evolution.

Author summary

The Spike of SARS-CoV-2 has accumulated many mutations during its time in circulation, most of which have occurred in the S1 region, and more specifically in the RBD, in an effort to either improve the virus's affinity for the receptor ACE2 or to enhance its

JSGG20200225152008136 and JCYJ20190807154603596 to YQC, JCYJ20200109142438111 and GXWD20201231165807008 to YM, KQTD20200820145822023 to MS). The funders had no role in study design, data collection and analysis, decision to publish, or preparation of the manuscript.

Competing interests: The authors have declared that no competing interests exist.

ability to evade the immune system. Mutations in the Spike S2 region have more far-reaching effects than those in the S1 region because it is more conserved across *Sarbecoviruses*. By comparing SARS-CoV and SARS-CoV-2, we found that an important substitution at amino acid position 813 in the S2 region (T813S) disrupts the utilization of TMPRSS2 and can significantly influence viral entry into cells. This discovery deepens our knowledge of S proteins and provides new prospects for tracing the evolution of *Sarbecoviruses*.

Introduction

Since its outbreak, SARS-CoV-2 has caused hundreds of millions of illnesses cases and fatalities globally, making it by far the worst public health catastrophe of the 21st century [1]. SARS-CoV-2 was the seventh human coronavirus and likely originated in a bat host [2,3], belonging to the *Sarbecovirus* subgenus of β-coronaviruses [3,4], along with SARS-CoV, which caused an outbreak in 2002–2003 [5]. Spike (S), as the surface glycoprotein, facilitates virus' cell entry through host receptor binding with its S1 subunit (S1) and membrane fusion mediated by its S2 subunit (S2) [6,7]. The receptor-binding domain (RBD) is located towards the C-terminus of S1 and is responsible for binding to the receptor, angiotensin-converting enzyme 2 (ACE2) [8,9]. RBD is the primary focus of vaccine designing [10–12] and neutralizing antibody screening [13–15] despite being highly genetically variable among variants [16–18]. After spike binding to ACE2, conformational change of S2 is triggered and this conformational change facilitates fusion between the viral and host cell membranes [19], this process is believed to be highly modulated by proteolysis.

Spike protein contains multiple proteolytic sites, while a single arginine is usually located at the S1/S2 boundary and susceptible to trypsin-like protease cleavage. It is unique among *Sarbecovirus* spikes that SARS-CoV-2 S contains a multi-basic cleavage site (681-PRRAR-685), between the S1 and S2 subunits [20]. It has been proposed that cleavage at the S1/S2 site facilitates S priming and promotes membrane fusion but is not essential to membrane fusion [21]. Spike S2 contains a S2' site for cellular protease cleavage [22,23]. It has been proposed that the S2' site must be cleaved to fully initiate the fusion process, by either transmembrane serine protease 2 (TMPRSS2) [24] on the cell surface or by cathepsin L (CTSL) [25] in the endosomes. S2 consisted of 3 key motifs for membrane fusion: fusion peptides (FPs) and heptad repeat 1 (HR1) and 2 (HR2). HR1 and HR2 form a six-helix bundle fusion core in post-fusion S [26]. FPs are pivotal in viral entry and highly conserved between β-coronaviruses [22]. However, the exact sequence of "fusion peptide" has not yet been determined [27–30]. In a previous study, two FP candidates have been identified based on cleavage sites [27], FP1 (Amino acid (AA) 788–806) located behind S1/S2 and the extremely conserved FP2 (AA815-833) located behind S2' site.

The membrane fusion process is crucial to viral infection. Despite sharing about 76.47% amino acid identity on S protein [31], SARS-CoV and SARS-CoV-2 have generated extremely distinct infection events: The SARS-CoV-2 pandemic has lasted for more than three years and the virus is likely to remain circulating. In contrast, the 2003 SARS-CoV world-wide outbreak was quickly eradicated. The exact reason for the transmissibility difference between the two related viruses is likely to be complex and yet to be understood. The ability to use ACE2 efficiently has been proposed to be a key prerequisite for viral infection [32]. It has been reported that SARS-CoV-2 S binds to ACE2 with 10- to 20-fold higher affinity than SARS-CoV S [33], but another study showed similar affinities between SARS-CoV and SARS-CoV-2 RBD

binding with ACE2 [20]. Although receptor binding is an essential step for virus cell entry, the subsequent S2 mediated membrane fusion is also essential [7]. In this study, we investigated the fusogenic activities of S2 using a split-GFP system, and we found that SARS2 S2 mediates more robust membrane fusion than SARS S2. We further demonstrated that the threonine to serine substitution at residue 813 in S2 significantly enhance membrane fusion and probably enhance the spread of *Sarbecovirus*.

Results

SARS-CoV-2 S2 induces more syncytia formation than SARS-CoV S2

To investigate the role of S2 in SARS-CoV-2 infection, we constructed a chimeric SARS-2-S protein bearing SARS-CoV S2 (cSARS2-S2sars, spike2), and a chimeric SARS-S protein bearing SARS-CoV-2 S2 (cSARS-S2sars2, spike4) (Fig 1A). Flow cytometry experiments were performed to detect the surface expression levels of S proteins, and the results showed that there was no difference between the chimeric S and their parents (Fig 1B and 1C). Western blot (WB) was performed to compare cleavage efficiency of these proteins by quantifying the band intensity of CL-S and FL-S to monitor S2 formation, and the results showed that there was no significant difference in S2 formation between chimeric S and their parents regardless of trypsin treatment (Fig 1D down). In addition, we observed that the cleavage efficiency of SARS-CoV-2 S was higher than that of SARS-CoV S, which lacks PRRAR and cannot be cleaved by furin during synthesis, but trypsin treatment increased the cleavage of SARS-CoV S significantly (Fig 1D). In the following membrane fusion assays, we treated all S proteins expressed on cells with trypsin to improve the sensitivity of fusion assays and enable a more precise characterization of the impact of key site mutations, similar to those reports about the fusogenicity of SARS-CoV S2 [34] or FPs [35].

To assay the membrane fusion activities of these chimeric S proteins, we utilized a green fluorescent protein (GFP)–Split complementation system [36,37], in which GFP is split into two non-fluorescent parts, GFP1-10 and GFP11, and the reassembly of GFP1-10 and GFP11 reconstitutes a functional chromophore. With transfection, we introduced GFP1-10 and GFP11 into the donor cells transiently expressing various S proteins and the acceptor cells stably expressing ACE2 (hACE2), respectively. The spike-mediated fusion of donor and acceptor cells could lead to the formation of syncytia, and then GFP1-10 and GFP11 were present in the same intracellular environment and formed green fluorescence. The fluorescence from the chromophore reflects the fusion activities of these S proteins (Fig 1F). Two hours after the coculture of donor and acceptor cells, the cell fusion accompanied by the GFP was observed under microscopy, and the green fluorescence positive area increased rapidly with more cell fusion (Fig 1E). In this work, we quantified cell fusion activity by calculating the area ratio of GFP to DAPI. We observed that the rate and size of syncytium formation were affected by various S proteins. SARS-CoV-2 S was more effective at cell fusion than SARS-CoV S, which is consistent with their spread ability. Of note, we found the cell fusion ability of S proteins were mainly correlated with the S2. When replaced with SARS-CoV-2 S2, the fusogenicity of chimeric protein spike4 was remarkably improved compared with its parent, SARS-CoV; the fusion rate and size all increased; on the other hand, after replacing SARS-CoV S2, the chimeric protein spike2 lost most of its cell fusion ability, the fusion rate and size reduced significantly (Fig 1E and 1G). A direct visualization system was also used to monitor the number and size of syncytia formed by these proteins. After mixing with ACE2-293T cells 48 hours, we observed that the syncytia area of SARS2-S protein was the largest, and the swapped of SARS-CoV S2 reduced the size but increased the number; the syncytia of SARS-S protein was not obvious, but the chimera of SARS-CoV-2 S2 induced more but small size syncytia (Fig 1H).

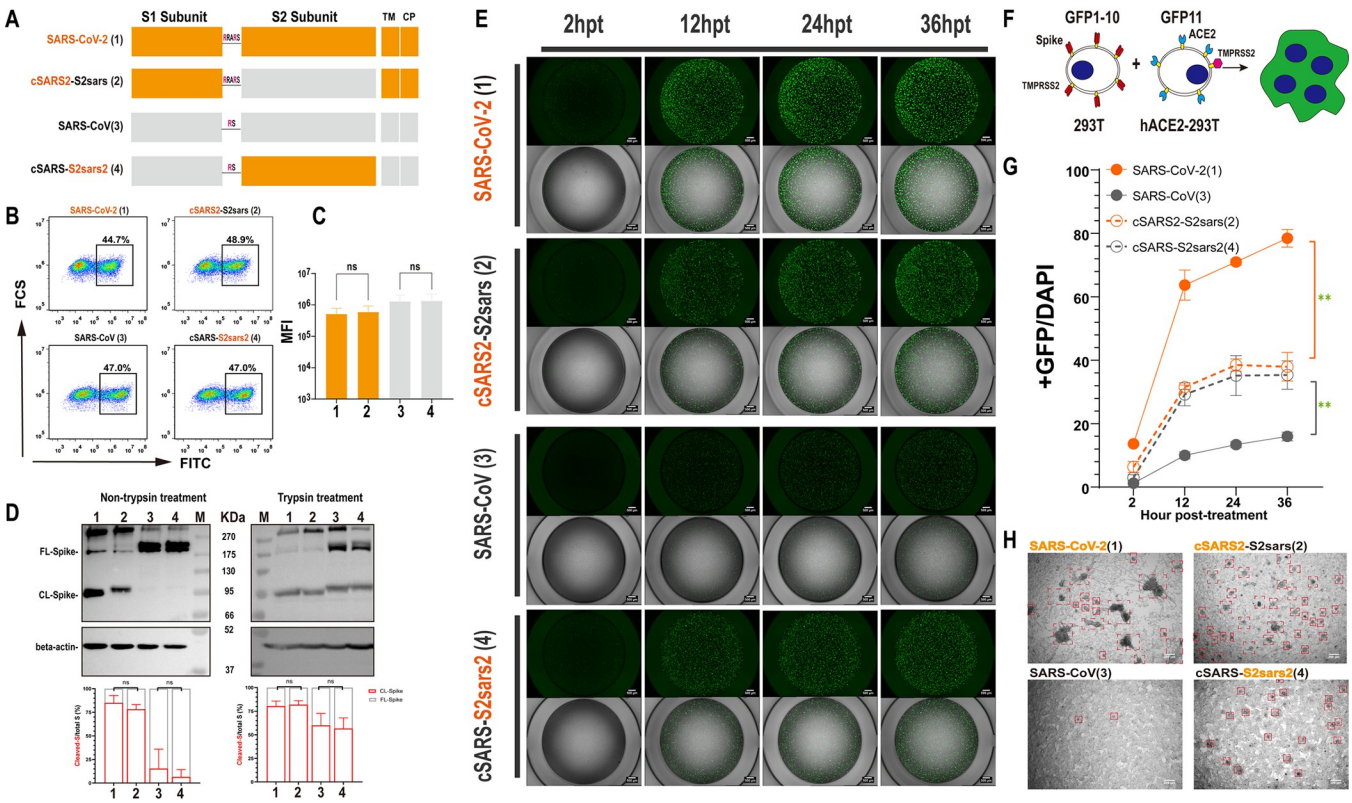

Fig 1. Replacement of S2 subunit affected the fusogenicity of S protein. (A) Schematic diagram for the construction of the S2-chimeric Spike. The Saffron graph depicts SARS-CoV-2 S, which has the multibasic motif (PRRAR) at the S1/S2 Cleavage Site; the grey graph represents SARS-CoV S. The numbers in parentheses are identical to those in Fig 1B–1G. TM, transmembrane domain; CP, cytoplasmic domain. (B and C) Flow cytometry. After transfection, the expression of surface S proteins was detected using s309 antibody which binds RBD efficiently and mouse anti-human IgG-FITC, respectively (B) and the summarized results are shown (C). MFI, mean fluorescent intensity. (D) Western blot. Representative blots of cell lysates showing spike cleavage in parental and chimeric Spikes with or without trypsin treatment. Immunoblots were probed with the C-terminal part of the spike protein detected by using an anti-Flag tag antibody, the full-length (FL) S and cleaved (CL) S (i.e., S2) were marked as indicated; Beta-actin was probed as a loading control. The band intensity was densitometrically calculated using Image J, and the ratio of Cleaved-S/total S (%) was shown to quantify the difference in the S2 formation. (E-G) Spike-based cell-cell fusion assay. A schematic diagram showing the GFP-split system for Spike-ACE2 mediated cell fusion (F), and representative images at 2, 12, 24, 36 h post-treatment (E). The summarized results of the ratio of fusion were shown (G). Scale bar, 500 μm. (H) Microscopic observation of syncytia. Cells expressing S proteins were photographed under a regular phase contrast light microscope with a 10× lens, and representative images at 48 h after mixing with ACE2-293T cells. Scale bar, 200 μm. Results are means +/- SD from at least three fields per condition. Results are representative of at least three independent experiments. Statistically significant differences between parental S (Spike1 or Spike3) and chimeric S (Spike2 or Spike4) were determined by a two-sided Student's t test (C and D, ns: non-significant), or two-sided paired t test (G, *: $p<0.05$, **: $p<0.01$).

https://doi.org/10.1371/journal.ppat.1011123.g001

Collectively, these results suggest that S2 plays an important role in SARS-CoV-2 infection, and its alternation could affect the fusogenicity of S protein significantly.

The Spike fusogenicity is dependent on the Internal Fusion Peptide (IFP)

To further identify key functional domains or motifs in S2 for increased spike fusogenicity, we divided S2 into three parts based on their functions [22,38] and constructed chimeric Spike5 (SARS-CoV F1, AA668-815), Spike6 (SARS-CoV F2, AA816-966), Spike7 (SARS-CoV F3, AA967-1195) and Spike10 (SARS-CoV-2 F1, AA686-833), Spike11 (SARS-CoV-2 F2, AA834-984), Spike12 (SARS-CoV-2 F3, AA985-1213) by directly replacing amino acids of the corresponding regions on Spike1 and Spike3, respectively, as shown in Fig 2A and 2G. Via Flow cytometry and WB assay, we confirmed no significant difference in cell surface expression of these S proteins (Fig 2B and 2H); and the unchanged CL-S ratio for most chimeric S, except for Spike 6, with increased cleavage; and Spike 5, with decreased cleavage (Fig 2C and 2D).

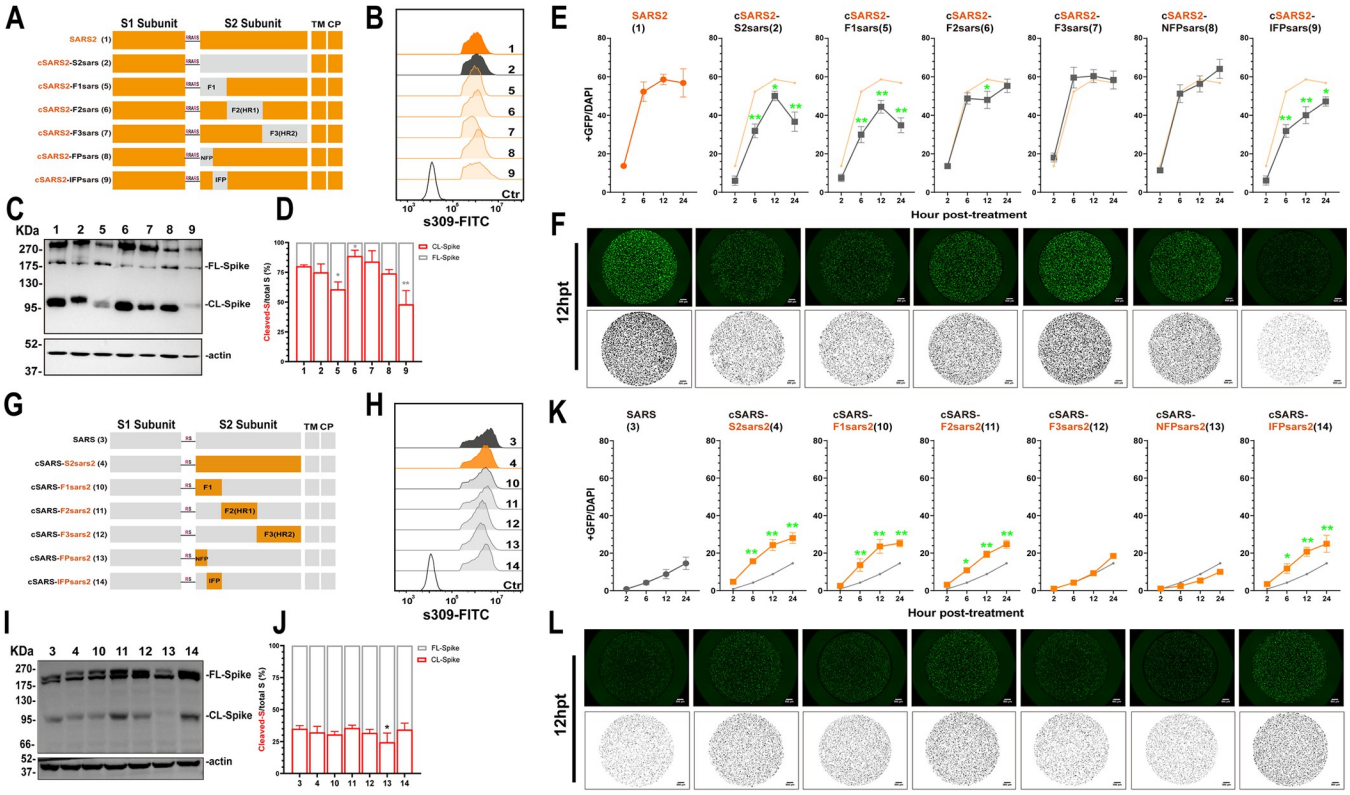

Fig 2. Replacing IFP motif of parental Spike influenced the fusogenicity significantly. (A and G) Schematic diagram of the S2-chimeric Spike bearing swapped motif. The S2 was divided into 3 parts according to the structure and function: F1 (686–833), F2 (834–984) and F3 (985–1213) of SARS-CoV-2 (A); F1 (668–815), F2 (816–966), F3 (967–1195) of SARS-CoV (F). Then replacing the corresponding parts with the others separately. Further, the F1 was divided into two parts: FP (686–787) and IFP (788–833) of SARS2 (A), or FP (668–769) and IFP (770–815) of SARS (F). The numbers in parentheses are identical to those in Fig 2B–2F and 2G–2L. (B and H) Flow cytometry. The summarized results of the surface S expression were shown. s309 antibody and mouse anti-human IgG-FITC were used respectively. (C, D and I, J) Western blot. A representative blot of cell lysates showing spike cleavage. FL-Spike and CL-Spike were marked as indicated. Beta-actin was used as a control. The band intensity was densitometrically calculated using Image J, and the ratio of Cleaved-S/total S (%) was shown. (E and K) Spike-based fusion assay. The fusion activity was quantified by measuring the ratio of GFP+ area to DAPI area by imaging at different times (2, 6, 12 and 24hpt). The results for SARS-CoV-2, Spike4, 10–14 were shown as Saffron lines and SARS-CoV, Spike2, 5–9 were shown as grey lines, respectively. (F and L) Representative images of cell-cell fusion. Scale bar: 500 μm. Results are means +/- SD from at least three fields per condition. Results are representative of at least three independent experiments. Statistically significant differences between parental S (Spike1 or Spike3) and chimeric Spikes were determined by two-sided paired t test (D and J, *: $p<0.05$, **:$p<0.01$), or Student's test at each point (E and K, *: $p<0.05$, **: $p<0.01$).

https://doi.org/10.1371/journal.ppat.1011123.g002

Subsequent membrane fusion assays showed that swapping of F1 regions significantly affected the fusogenicity of the chimeric S proteins. The area of GFP decreased after introducing SARS-CoV F1 into SARS2-S (Spike 5, Fig 2E and 2F), while GFP signal increased significantly when SARS-CoV-2 F1 was introduced into SARS-S (Spike 10, Fig 2K and 2L). The swapping of F2 and F3 between SARS-S and SARS2-S failed to produce a similar significant alternation in the fusogenicity of S proteins as F1.

We further divided F1 into two portions based on whether they contained FPs or not. We define the Non-Fusion Peptide (NFP) fragment at the N-terminus and the Internal Fusion Peptide (IFP) fragment at the C-terminus. IFP fragment contained FP1 and FP2. Following the similar abovementioned strategy for swapping mutant S proteins, we constructed following chimeric S constructs. We found that after swapping NFP (Spike8, SARS-CoV AA668-769; Spike13, SARS-CoV-2 AA686-787) and IFP (Spike9, SARS-CoV AA770-815; Spike14, SARS-CoV-2 AA788-833), the surface expression of chimeric S was the same as the parents (Spike1 and Spike3) (Fig 2B and 2H), while the cleavage ability had a difference. We found that

introducing SARS-CoV IFP into SARS2-S and introducing SARS-CoV-2 NFP into SARS-S could affect the expression of S protein and decreased spike cleavage respectively (Fig 2C, 2D, 2I and 2J), these results suggested direct motif replacement might affect the cleavage of S, and SARS-CoV-2 FP, especially IFP, might enhance the ratio of CL-S. Subsequent membrane fusion assays showed that IFP was the key factor of S fusogenicity, replacing SARS-CoV IFP alone to SARS-CoV-2 backbone (Spike9) was able to reduce S protein's membrane fusion capacity significantly and vice versa (Spike14) (Fig 2E, 2F, 2K and 2L). We also found that SARS-CoV-2 F2 fragment (Spike 11) promoted fusion and this might be related to the increased S expression.

To further validate the role of IFP in S fusogenictiy, we directly replaced fragments on Spike2 and 4 for chimeric plasmid construction (S1A and S1F Fig) and further assayed cell membrane fusion ability. We found that the surface expression (S1C and S1H Fig) and the CL-S ratio (S1B and S1G Fig) of most chimeric S was the same, except for the reduction in Spike20 and the enhancement of Spike19 and 22 (S1B and S1G Fig), this results further proved SARS-CoV-2 IFP enhanced the cleavage of S protein. The membrane fusion results showed that introducing SARS-CoV-2 F1 or IFP moderately enhanced the fusion ability of Spike2 (S1D and S1E Fig), but substitution of SARS-CoV F1 and IFP significantly inhibited the fusion ability of Spike4 (S1I and S1J Fig), these results confirmed that the backbone of chimeric protein might affect S fusogenicity, but IFP was the key fragment.

Collectively, these results showed that although there was some variation across chimeric S, IFP was the most critical factor affecting fusion.

IFP S813T mutation reduces the cell membrane fusion ability of SARS-CoV-2 S protein significantly

The IFP sequence is relatively conserved between SARS-CoV S and SARS-CoV-2 S, with only six different amino acids. To investigate whether these amino acids influence the fusogenicity of S protein, we investigated the impact of each amino acid on cell membrane fusion by introducing mutations on each of them in Spike9 (Fig 3A and 3F). WB and flow cytometry assays revealed no significant differences in expression and cleavage of each mutant S protein, except for Spike29, which is poorly expressed (Fig 3B and 3C). Subsequent membrane fusion assays revealed that only the T813S mutation significantly increased the chimeric protein's fusion capability (Fig 3D and 3E).

Similar experiments were performed on Spike14. The expressions and cleavages of all mutant, Spike31-36, were comparable to that of the parent S protein, spike14 (Fig 3G and 3H). Despite Spike31 (I788M) and Spike32 (P793T) showing mildly reduced fusion activities, subsequent experiments showed that only the S813T mutation reduced the membrane fusion properties of the S protein significantly (Fig 3I and 3J).

These findings corroborated that the mutation of serine to threonine on residue 813 dramatically reduced the fusion ability of chimeric S proteins, suggesting that residue 813 plays a pivotal role in SARS-CoV and SARS-CoV-2 S2 mediated-fusogenicity.

S813T mutation disturbes the *Sarbecovirus*'s membrane fusion and infection significantly

To further consolidate the above findings, we introduced S813T mutation in S proteins of SARS-CoV-2 and its variants of concern (VOC) strains (Spike37-41), and T813S mutation in SARS-CoV S protein. As shown in Fig 4A (red lines) and 4B (top panel), the membrane fusion activities of spikes with S813 (S813 S) were significantly higher than those spikes with T813 (T813 S) in ACE2-293T cells. We also conducted the fusion assay in Caco-2 cells, a type of

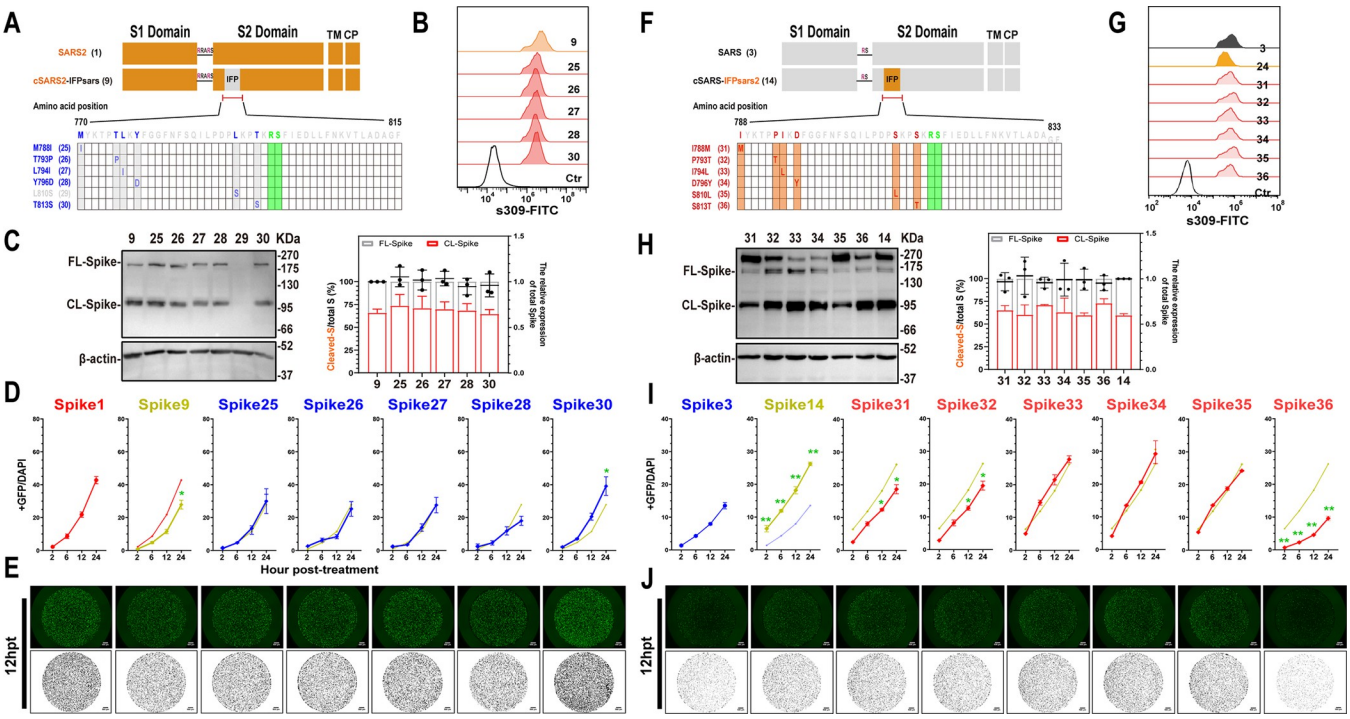

Fig 3. S813T mutation affected the cell membrane fusion ability of IFP-chimeric Spike. (A and F) Schematic diagram of the IFP-chimeric Spike mutants and the numbers in parentheses are identical to those in Fig 3B–3D and 3G–3I. Align the sequence of AA 788–833 in SARS-CoV-2 with SARS-CoV (AA 770–815). Residue numbering is shown according to SARS-CoV-2 S. The mutation sites were marked in red or blue, and the S2' cleavage sites were in Green. (B and G) Flow cytometry. The summarized results of the surface S expression were shown. s309 antibody and mouse anti-human IgG-FITC were used respectively. (C and H) Western blot. Left panel: A representative blot of cell lysates from WT and mutant chimeric-Spike expressing 293T cells, FL-Spike and CL-Spike were marked as indicated. Beta-actin was used as a control. Right panel: quantified band intensity using Image J to analyze the protein expression and the ratio of Cleaved-S to the total S. (D and I) Spike-based fusion assay. The fusion activity was quantified by measuring the ratio of GFP+ area to DAPI area by imaging at different times (2, 6, 12 and 24hpt). The results for mutant Spike9 and 14 were shown as yellow-green, Spike25-30 as blue lines, and Spike31-36 as red lines, respectively. (E and J) Representative images of cell-cell fusion. Scale bar: 200 μm. Results are means +/- SD from at least three fields per condition. Results are representative of at least three independent experiments. Statistically significant differences between parental S (Spike9 or Spike14) and mutants were determined by Student's test at each point (D and I, *: $p<0.05$, **: $p<0.01$).

https://doi.org/10.1371/journal.ppat.1011123.g003

small intestinal epithelial cells that naturally express high levels of ACE2 and TMPRSS2 [39,40]. Our results showed a higher fusion ability in Caco-2 cells, but the S813T mutation disrupted fusogenicity in a similar manner (Fig 4A (green lines) and 4B (bottom panel)). The flow cytometry assay confirmed no significant difference in the expression of various S proteins (Fig 4C). Despite variations in S protein cleavage levels between strains and obvious enhancement of S2 formation with trypsin treatment, we observed that S813 S and T813 S of a given strain had roughly the same level of cleavage, with only S813 S of SARS-CoV-2 and Delta (with or without trypsin), T813 S protein of SARS-CoV (with trypsin) having noticeably stronger levels of cleavage than their counterparts (Fig 4D). This suggests that the enhancement of membrane fusion by T813S likely stems from a mechanism independent of S1/S2 cleavage.

Considering the pivotal role of T813S substitution in the membrane fusion properties of the S protein, we next interrogated its possible role in viral infection. We rescued single-cycle infectious coronavirus-like viral particle by coexpressing the SARS-CoV-2 replicon [41] and various S genes in package cells, similar to those developed in previous studies [42,43]. The viruses with various S proteins were used to infect ACE2-293T and Caco-2, and the replication products, subgenomic RNAs, were quantified with RT-qPCR. As shown in Fig 4E, the

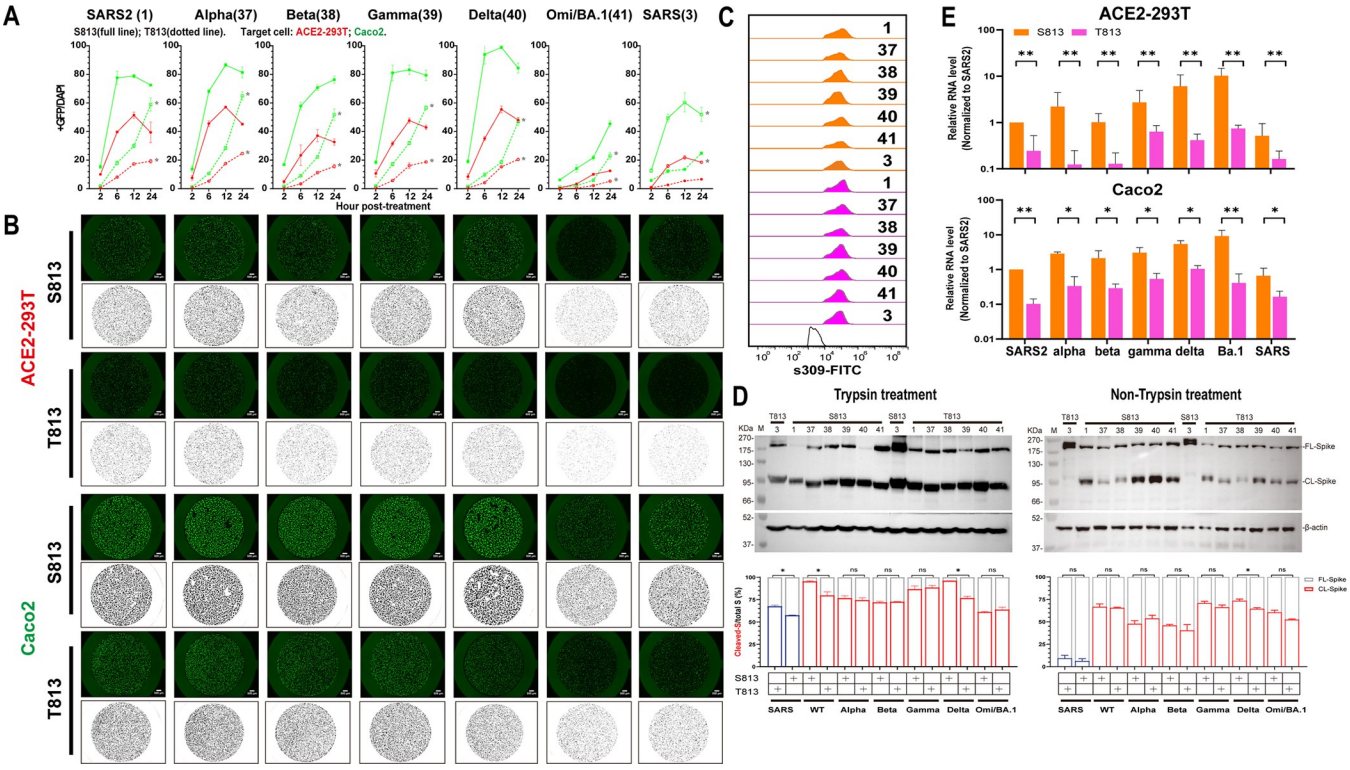

Fig 4. Spike S813T mutation disturbed the membrane fusion and infection of *Sarbecovirus* significantly. (A) Spike-based fusion assay. The fusion activity was quantified at different times (2, 6, 12 and 24hpt). ACE2-293T (Red) and Caco-2 (Green) were used, the results of S813 Spike were shown as full lines and T813 Spike as dotted lines. (B) Representative images of cell-cell fusion. Scale bar: 200 μm. (C) Flow cytometry. The summarized results of the surface S expression were shown. s309 antibody and mouse anti-human IgG-FITC were used. S813 S and T813 S were shown as saffron and magentas, respectively. (D) Western blot to monitor the S2 formation with or without trypsin treatment. Top panel: A representative blot of cell lysates from S813 and T813 Spike expressing 293T cells, FL-Spike and CL-Spike were marked as indicated. Beta-actin was used as a control. Bottom panel: quantified band intensity using Image J to analyze the protein expression and the ratio of Cleaved-S to the total S. (E) Pseudovirus assay. The replication of Pseudovirus with S813 or T813 Spike in ACE2-293T and Caco-2 cells was determined by RT-qPCR, and the infectivity percentage normalized with that of the virus pseudotyped with Spike1 was shown. S813 S and T813 S were shown as saffron and magentas, respectively. Results are means +/- SD from at least three fields per condition. Results are representative of at least three independent experiments. Statistically significant differences (*: $p<0.05$) between S813 S and T813 S were determined by Student's test at each point (A), or two-sided paired t test (D and E).

https://doi.org/10.1371/journal.ppat.1011123.g004

transduction activity of the mutant with S813 S was significantly higher than that of T813 S in SARS-CoV-2, SARS-CoV, or VOC strains. These results indicated that S813T can affect virus entry by modulating the membrane fusion properties of S protein.

The S813T mutation has no effect on S protein interactions with ACE2

To investigate how S813T mutation alters S fusogenicity, we used a competitive ELISA assay to examine the role of residue 813 in interactions between S protein and ACE2. S813 S and T813 S was separately expressed firstly (Fig 5A). In our study, SARS-CoV-2 S contained six proline substitutions to generate stabilized and soluble prefusion form [44–46]; SARS-CoV S also contained two stabilizing proline mutations in S2 subunit according to an effective stabilization strategy [47,48]. The results showed that S813 S and T813 S proteins had similar affinities towards the ACE2 receptor, indicating that S813T mutation had no effect on S protein receptor binding (Fig 5B). We further verified this finding by assessing the neutralization of RBM-targeting antibodies, which directly blocked the interaction between S protein and ACE2. In this study, we used antibody m396 [49] for SARS-CoV, and X65 [14] for SARS-CoV-2; we found that the representative antibodies showed similar neutralization efficiencies against

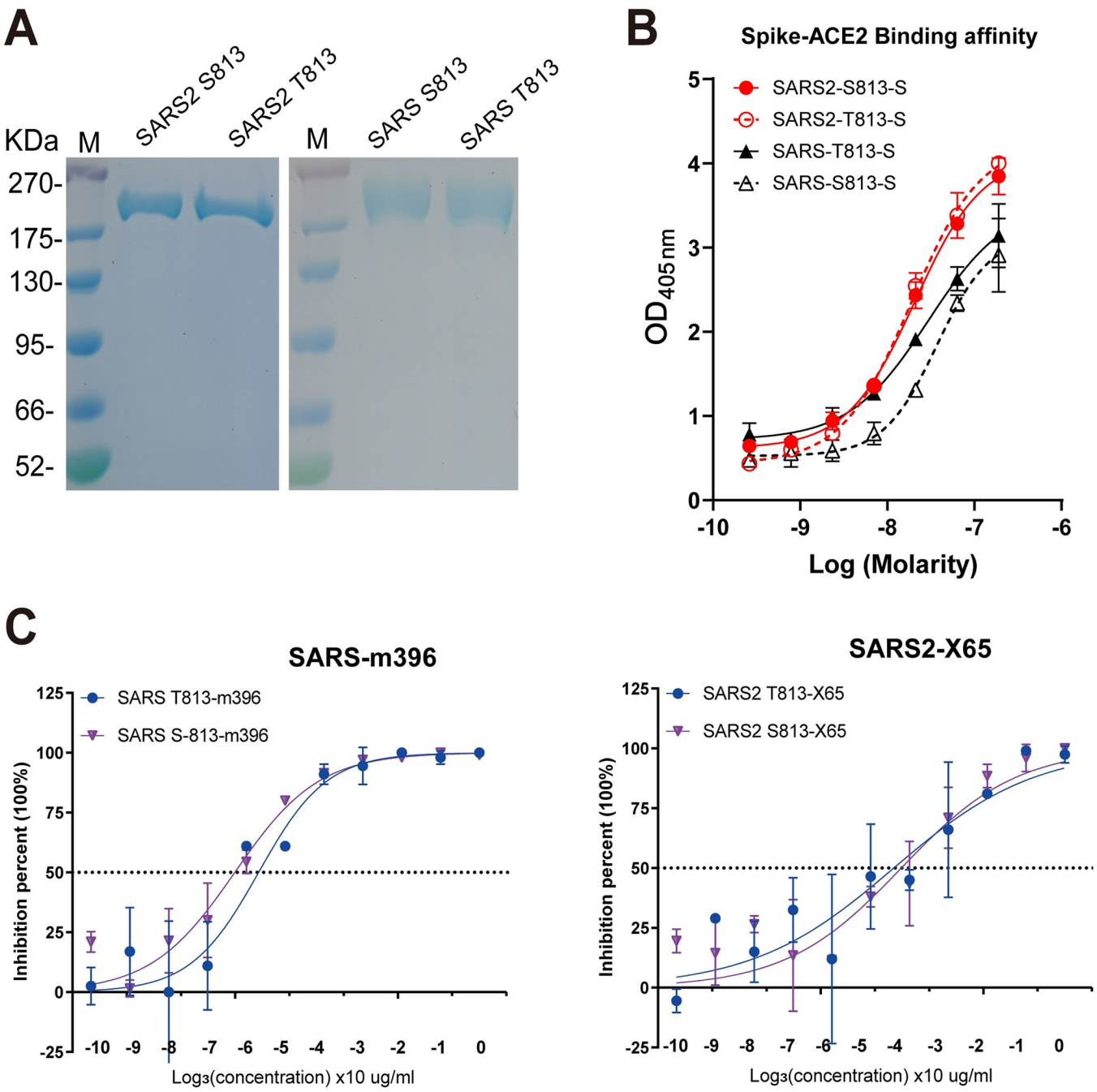

Fig 5. The S813T mutation has no effect on S protein interactions with ACE2. (A) SDS-polyacrylamide gel electrophoresis (PAGE) of SARS2-6P, SARS-2P and Residue 813 substitution S variants. Molecular weight standards are indicated at the left in KD. (B) Competitive ELSIA to detect the binding affinity between S proteins and ACE2. Red line indicated SARS-CoV-2, and blue line indicated SARS-CoV. (C) Neutralization curves for RBD representative antibodies, m396 and X65, with the VSVpp containing parent and mutant S proteins. Each point represents the mean and standard error of 2 independent measurements.

https://doi.org/10.1371/journal.ppat.1011123.g005

VSV particles pseudotyped (VSVpp) with parental and mutant S proteins (Fig 5C). In summary, we confirmed that the S813T mutation did not affect S protein interactions with ACE2 and RBD antibodies.

S813T mutation reduces the use of TMPRSS2 by S protein

Proteolytic activation of S is critical in the process of CoV entry into cells [50]. It has been reported that efficient infection of SARS-CoV and SARS-CoV-2 requires sequential cleavage of S by furin at the S1/S2 site and then by TMPRSS2 at the S2' site or by CTSL at two specific sites [51] in endosome when TMPRSS2 expression is repressed (Fig 6A). We noticed that S2' site is highly conserved in *Sarbecovirus* spikes and residue 813 is located in close proximity to the S2' site, highly conserved in *Sarbecovirus* spikes, and therefore the 813 change could potentially affect cleavage by TMPRSS2.

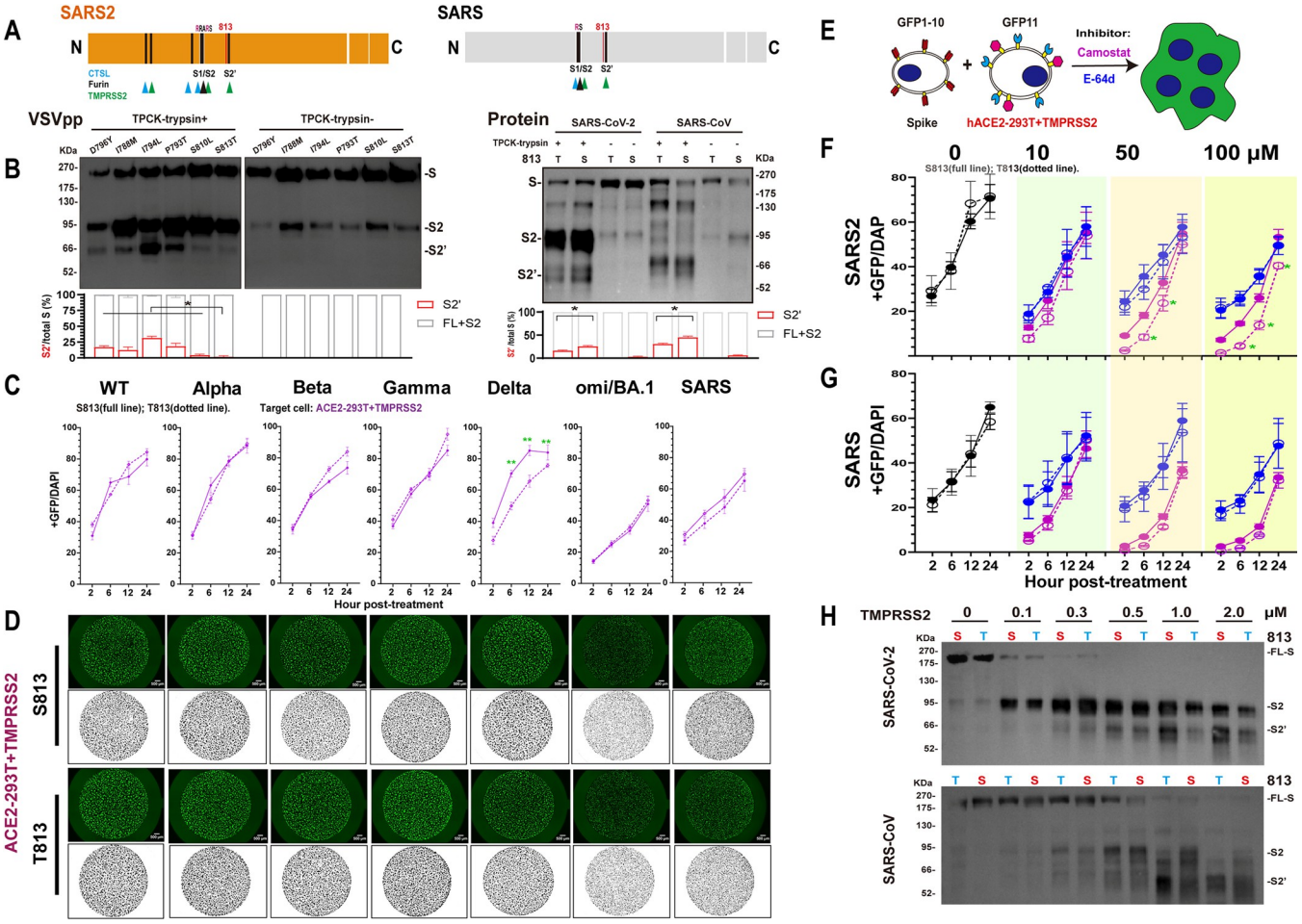

Fig 6. S813T mutation reduced the use of TMPRSS2 by S protein. (A) Schematic illustration of SARS-CoV S and SARS-CoV-2 S including proteolytic cleavage sites: S1/S1, S2' and CTSL cleavage sites in S1. Residue 813 was indicated as red. Arrow heads indicated the cleavage site. (B) Western blot. Top panel: A representative blot of VSVpp digested with TPCK-trypsin (2 μg/ml at 37˚C for 30 min), FL-Spike (S) and CL-Spike (S2 and S2') were marked as indicated. Bottom panel: quantified band intensity using Image J to analyze the protein expression and the ratio of S2 and S2' to the total S. (C) Spike-based cell-cell fusion assay. With the overexpression of TMPRSS2 (purple) in ACE2-293T, the fusion activity was quantified at different times (2, 6, 12 and 24hpt). The results of S813 S were shown as full lines and T813 S as dotted lines. (D) Representative images of cell-cell fusion. The area of cell fusion was shown as green (up) and black (bottom). Scale bar: 500 μm. (E-G) Fusion inhibition of Camostat and E-64d in ACE2-293T+TMPRSS2. A schematic diagram showing the GFP-split system with the inhibitor Camostat and E-64d for Spike-ACE2/TMPRSS2 mediated cell fusion (E). After being pre-incubated with the indicated concentration (0, 10, 50, 100 μm) of Camostat (F) and E-64d (G), the fusion activity was quantified at different times (2, 6, 12 and 24hpt), and the results of Camostat were shown as purple and E-64d as blue. (H) Spike cleavage assay by TMPRSS2. A representative blot of SARS-CoV-2 (Up panel) or SARS-CoV (Down panel) Spikes digested with TMPRSS2 at 0, 0.1, 0.3, 0.5, 1.0, 2.0 μM in assay buffer, at 37˚C for 30 min, FL-Spike (S) and CL-Spike (S2 and S2') were marked as indicated. Results are means +/- SD from at least three fields per condition. Results are representative of at least three independent experiments. Statistically significant differences (*: $p<0.05$) between S813 Spike and T813 Spike were determined by Student's test at each point (C, F and G).

https://doi.org/10.1371/journal.ppat.1011123.g006

To test this hypothesis, we investigated the impact of S813T mutation on the S2' site cleavage on VSVpp and S proteins by TPCK-trypsin, the serine protease domain of which has extremely high homology with TMPRSS2 [52] and previous studies have used it to observe the S2' formation [53,54]. WB analyses showed that S813T mutation had the most significant effect on S2' cleavage compared with other point mutations in IFP (Fig 6B left). What's more, as shown in the right panel of Fig 6B, the S2' formation of S813 S was more effective than T813 S, both in SARS-CoV and SARS-CoV-2; and the S1/S2 cleavage increased in SARS-CoV-2 but not in SARS-CoV significantly. Additionally, we found that the cleavage bands between S813 S and T813 S were significantly different, indicating that the T813S mutation may have altered SARS-CoV S cleavage.

At the same time, we overexpressed TMPRSS2 in ACE2-293T cells firstly (S2C Fig) and then used the GFP-split system to compare the fusion activities of S813 S and T813 S. We found membrane fusion activities of S813 S and T813 S increased with increasing level of TMPRSS2 expression and both plateaued to similar levels (S2A and S2B Fig), this phenomenon was observed for most VOC strains, with only Delta S813 S being stronger than T813 S (Fig 6C and 6D), indicating that increasing TMPRSS2 expression restored the S813T mutation to interfere with S proteins, in other words, the S813T mutation likely reduced S protein sensitivity to TMPRSS2.

To further investigate this possibility, we used the TMPRSS2-specific inhibitor Camostat and examined its effect on membrane fusion under various concentrations, the results (Fig 6E–6G) show that when Camostat concentration was low (10 μM), there was no discernible difference in the ability of S813 S and T813 S in the ACE2-293T/TMPRSS2 system; however, when the Camostat concentration was increased, the difference gradually became apparent, eventually showing that S813 S was significantly higher than T813 S (Fig 6E and 6F). The effect of CTSL inhibitor E-64d was also tested and the results revealed that it had a modest, concentration-independent inhibitory effect in the ACE2-293T/TMPRSS2 system, but did not affect the fusion ability between S813 S and T813 S, suggesting the effect of CTSL on S protein activation was diminished in the presence of TMPRSS2. In addition, we also made a direct cleavage of S proteins by TMPRSS2. The cleavage of TMPRSS2 was enhanced with concentration, and S2' bands of S813 S were more obvious than T813 S, especially at higher TMPRSS2 concentrations. We also found that the cleavage of SARS-CoV-2 S by TMPRSS2 was more efficient than SARS-CoV S, the enhancement of T813S mutation on S2' formation could be observed at 0.5 μM in SARS-CoV-2 S, while at 2 μM in SARS-CoV (Fig 6H).

Based on these results, it is suggested that the S813T mutation has an effect on S proteins fusion pathway modulated by TMPRSS2 by reducing TMPRSS2 cleavage at the S2' site. S813 S protein had higher utilization and could complete cleavage under low TMPRSS2 conditions; whereas the T813 S protein used lower and required increased amounts of TMPRSS2 to complete cleavage.

Evolution AA 813 on Spike in *Sarbecovirus*

Considering the significance of residue 813 in the S protein activation process, we reconstructed an evolutionary tree using the S protein sequences of representative SARS-CoV, SARS-CoV-2 and SARS-relative (SARSr) strains to observe their evolutionary trends in *Sarbecovirus*. At position 813, we observed only threonine and serine; threonine was almost only present in two major lineages of SARSr strains, including human SARS-CoV and related viruses; while serine was found in human SARS-CoV-2 strains, bat and pangoline associated SARS-like strains related to SARS-CoV-2 (such as RaTG13 discovered in 2013 and SL-CoVZXC21 discovered in 2015), as well as a lineage basal to all members of *Sarbecovirus*

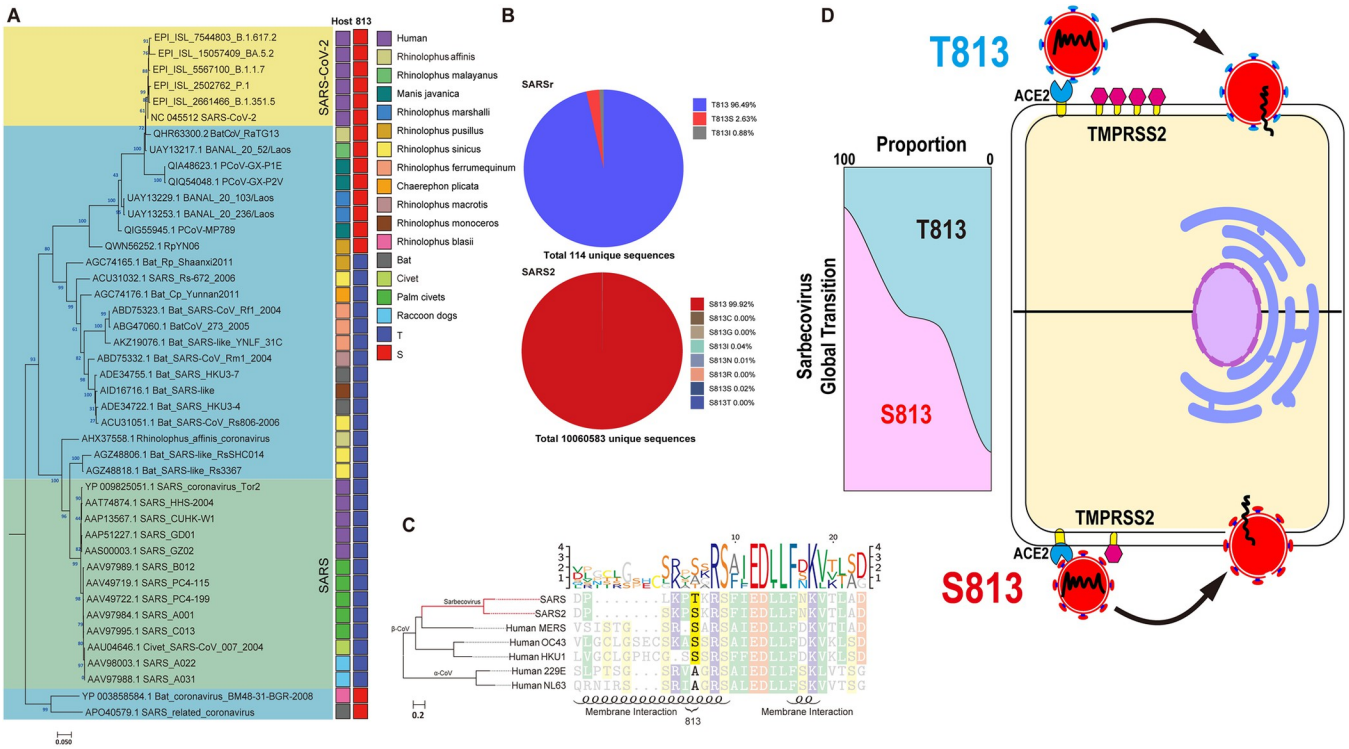

Fig 7. Genomic description of AA 813 in Spike of *Sarbecovirus*. (A) The phylogenetic tree based on *Sarbecovirus* S proteins (SARS-like strains, n = 24 genomes; SARS-CoV strains, n = 13 genomes; SARS-CoV-2 strains, n = 6 genomes). All strains invariantly containing serine at position 813 were marked red while containing threonine were marked mazarine. Color coding as indicated according to species. (B) Amino acid frequency of site 813. 114 complete spike protein sequences of SARS-CoV were collected from NCBI and 10,060,583 complete spike protein sequences of SARS-CoV-2 (2020–2022) were collected from GISAID. The method of analysis was performed as previously described [74]. Briefly, After removing redundant sequences with 100% sequence identity and multiple sequence alignment (MSA), site 813 based on the reference sequence of SARS-CoV-2 was derived and the amino acid frequency of site 813 can be calculated based on the un-redundant dataset of SARS-CoV and SARS-CoV-2, respectively. (C) Phylogenetic tree of Human coronavirus. The representative strains of 7 human coronaviruses were clustered by amino acid sequence phylogeny and observed the diversity of AA 813. In α-CoV (229E and NL63), there was only Alanine, while in β-CoV, Serine was in SARS-CoV-2, MERS-CoV, OC43-CoV and HKU1-CoV; threonine only in SARS-CoV. We used the WAG+F+I+G4 optimal model of the Iqtree software to construct a phylogenetic tree based on S proteins. The right-hand sequence mapping was based on texshade software for mapping. The secondary structure, i.e. the membrane fusion region, was predicted using the PSIPRED web page. (D) Schematic summary. By modifying the usage of TMPRSS2, Spike residue 813 affects the fusogenicity of *Sarbecovirus*. S813 S has a high utilization and complete the membrane fusion process with a small amount of TMPRSS2, but T813 S has a low ability and needs more TMPRSS2.Although both Serine and Threonine can be found at position 813, the evolutionary trend of Sarbecovirus maybe likely Serine.

https://doi.org/10.1371/journal.ppat.1011123.g007

(Fig 7A). Meanwhile, the mutation frequency of the amino acid at position 813 was calculated with 114 unique SARSr sequences and 10060583 unique SARS-CoV-2 sequences (GISAID 2020–2022.5.31), respectively. We discovered that in SARS-CoV, T813 accounted for 96.49% of the total and S813 accounted for 2.63%; however, in SARS-CoV-2, S813 accounted for as higher as 99.9%, while T813 accounted for only 0.01% (Fig 7B). Therefore, for SARS-CoV-2 T813 S was likely to be a random mutation that occurred in only a few individuals, without major sustained circulation in human population. Intriguingly, we discovered that other than SARS-CoV and related viruses, the rest of the β-cov, which included highly pathogenic MERS-CoV and SARS2, and the less pathogenic OC43-CoV and HKU1-CoV, were all predominantly serine (Fig 7C).

Discussion

SARS-CoV-2 had a substantially higher transmission capacity than SARS-CoV. Previous research has proposed that ACE2 binding efficiency [33] and polybasic cleavage site "PRRAR"

at S1/S2 boundary [30,55] were the primary causes. SARS-CoV and SARS-CoV-2 recognized the same receptor ACE2 in Humans. The previous study has shown that mutations in the SARS-CoV-2 RBD make it more accessible to the N-terminal end of ACE2 and stabilize two virus-binding hotspots at SARS-CoV-2 RBD/ACE2 interface [56]. The polybasic cleavage site of SARS-CoV-2 has been demonstrated to act as a determinant of transmission [57], and found that the site sensitized SARS-CoV-2 S protein to fusion-activating proteolysis during virus-cell entry [58]. In this study, we examined the membrane fusion activity of chimeric proteins with various S2s. Our results showed that the activity of S proteins bearing SARS-CoV-2 S2 is significantly higher than that bearing SARS-CoV S2, suggesting that alternation of S2 is sufficient to change the membrane fusion activity of S proteins without disturbing the RBD/ACE2 interaction. We narrowed down the functional domains of S2 to IFP, which is essential for the membrane fusion activity of S protein. Furthermore, we identified the key residue serine 813, as indicated by the data that a single mutation of T813S in SARS-CoV S protein could enhance membrane fusion in cell-based membrane fusion assays and viral entry in a single-cycle infectious SARS-CoV virus system.

Residue 813 is located immediately upstream of S2' site (Fig 3A and 3F) and is conserved in various coronavirus strains (Fig 7C). A recent study proposed that the replication-competent VSVΔG-SARS-CoV-2 S harbors the S813Y mutation, which reduced the enzymatic activity of TMPRSS2 and increased the stability of S protein for better vaccine design [53]. This unexpected discovery was in agreement with our finding and highlighted the importance of S813 in S protein fusion activity. However, it should be noted that S813Y mutation is not observed in known viral genomic sequences. In contrast, S813 and T813 used in our study are from the SARS-CoV-2 and SARS-CoV sequences, respectively. Thus, our findings were relevant to understanding the real function role of residue 813 during viral entry into the cell.

The fusogenicity of Spike is also affected by the ability of S2 formation, which was cleaved by endogenous furin or exogenous trypsin at the same site. The cleavage of SARS-CoV S by furin is poor and the S2 band can only be detected after trypsin treatment (Fig 1D 3, 4), which significantly reduced fusion sensitivity (S3 Fig). SARS-CoV-2 S contains the multiple basic cleavage sites PRRAR, and the S2 band can be observed regardless of trypsin treatment (Fig 1D 1, 2). Fusion assay shown that pretreatment without trypsin does not affect SARS-CoV-2 S fusogenicity and the difference between S813 S and T813 S (S3 Fig), indicating that trypsin treatment does not affect the reliability of the conclusions of this study.

Host proteases, including furin, TMPRSS2, and CTSL work together to modulate coronavirus S protein-mediated cell fusion [8], and disturbing the activity of these proteases will effectively inhibit virus infection and proliferation. Current research has revealed that TMPRSS2 inhibitors are superior to endocytosis inhibitors at preventing viral infection in human primary nasal epithelium. This may imply that TMPRSS2 is more crucial for viral entrance into respiratory cells than clathrin-mediated endocytosis [59]. TMPRSS2 is a type II transmembrane protein with serine protease activity and is required to trigger cell-cell fusion, it has been reported that TMPRSS2 knock-out 293T cells are unable to form syncytia [21]. TMPRSS2 has been proved to have stronger proteolytic activity against SARS-CoV-2 S than SARS-CoV S. A study has shown that this is due to the multibasic site at S1/S2 boundary, when introduced it into SARS-CoV S or ablated it from SARS-CoV-2 S, the difference can be diminished [7,60]. Here we found that the S2 also affected the utilization of TMPRSS2, the cleavage activity of TMPRSS2 on S813 S was significantly higher than that of T813 S in both SARS-CoV and SARS-CoV-2, and the effect of S813T mutation decreased with increased TMPRSS2 expression. Our data suggested that residue 813, in addition to the multibasic site at S1/S2, could somewhat affect the activity of TMPRSS2 on S protein (Fig 7D).

Our study demonstrates that S813T mutation affects the usage of TMPRSS2, but does it impact the function of Furin and CTSL? Furin is ubiquitously expressed in cells [61] and for SARS-CoV-2 S the cleavage site is located in the S1/S2 boundary [21]. Recently, a study found that K814A mutation significantly reduced furin-mediated cleavage of SARS-CoV-2 S and antagonized pseudovirus transduction, while the S813A had no effect [62]. This work suggests that residue 813 is unlikely to affect furin cleavage. CTSL is a member of the lysosomal cysteine protease and was highly expressed in most human tissues, including the respiratory system, gastrointestinal tract, kidney, and urogenital system [63]. Previous studies have shown that CTSL played a role in the proteolysis of SARS-CoV S [64,65] and SARS-CoV-2 S [25], and the cleavage site of CTSL in SARS-CoV S was at (near) S1/S2 [64], while in SARS-CoV-2 S, it was at two distinct conserved locations in the S1 subunit [51], suggesting residue 813 did not affect CTSL cleavage.

Our study also revealed that the F2 fragment, which includes HR1 (AA912-984) and a sheet-helix 4-helix 5 fragment (AA834-911), demonstrated some degree of fusion promotion (Fig 2). HR1, a critical component of six-helical bundle (6HB) formation, has a considerable influence on membrane fusion. In SARS-CoV-2, there are 19 amino acid substitutions compared to SARS-CoV, nine of which are located in HR1, with eight situated within the HR1 core site. According to previous reports, the HR1 of SARS-CoV-2 exhibits significantly greater helical stability and can more efficiently interact with the HR2 site to form 6HB [66].

SARS-CoV-2 is a fast-evolving virus, with rapid nucleotide substitution and recombination to generate new strains of altered virulence [67]. A most well-known example was the SARS-CoV-2 D614G strain rapidly replaced the original virus strain and became the dominant variant [68]. Further studies showed that D614G substitution favored an open conformational state of S protein [69] and promoted syncytium formation through enhanced furin-mediated S cleavage [70]. Through phylogenetic analysis of representative Sarbecovirus S sequences from SARS-CoV outbreak in 2002 to the emergence of COVID19 in 2022, we determined that threonine and serine are the only two potential amino acids at position 813 in Sarbecovirus, however, T813S mutation enhanced the S protein membrane fusion function, which might be likely leading to the emergence of SARS-CoV-2 in nature.

In summary, our study demonstrated that residue 813 was a key determinant of S protein fusogenicity and infectivity. The selection and increasing frequency of S813 S following the evolution of Sarbecovirus suggested that the T813S mutation was associated with an improvement of viral fitness through an increased S protein processing and fusogenic potential. These findings have important implications for understanding of the viral S fusogenicity.

Materials and methods

Cells and agents

Human embryonic kidney 293T (HEK293T) cells were maintained in Dulbecco's modified Eagle's medium (DMEM, Gibco) supplemented with 10% fetal bovine serum (FBS), 100 units/ml penicillin, 100 μg/ml streptomycin, and 2 mM L-glutamine. HEK293T cells that stably express human ACE2 (ACE2-293T) were cultivated in the presence of 2 μg/ml puromycin (Invivogen). Caco-2 (human epithelial colorectal adenocarcinoma) cells were cultivated in DMEM (Gibco) containing 20% FBS (TransGen Biotech), 100 μg/ml streptomycin (biosharp), 100 U/ml penicillin (biosharp), 1 mM Non-essential amino acids (NEAA, Gibco). All Cell cultures were incubated at 37˚C and 5% CO_2.

Plasmids

The pcDNA3.1(+) plasmid backbone was appended with a FLAG-tag sequence (DYKDDDDK) at the C-terminal. The spike coding sequences were all codon optimized for

human cells. For the construction of recombinant S plasmids. S2 subunit of SARS-CoV and SARS-CoV-2 VOC strains were amplified by PCR and appended with other regions of the target spike backbone to facilitate In-Fusion cloning.

pQCXIP-BSR-GFP11 and pQCXIP-GFP1-10 were from Addgene (68715,68716); Human TMPRSS2 was amplified from Caco-2 cells and cloned into pcDNA3.1(+) with a C-terminal FLAG-tag. All DNA constructs were verified by Sanger sequencing (ACGT).

Flow cytometry

We conducted Flow cytometry using a Beckman CytExpert (Beckman) and data was analyzed with FlowJo software. 293T cells transfected with S proteins for 36h were performed in PBS with 1% BSA. Cells were incubated with primary antibodies on ice for 1h and washed twice with PBS, then incubated with FITC goat anti-human IgG(H+L) (Southern Biotechnology Associates,1:400) for 45 min on ice. Transfection efficiency was assessed by staining with SARS-CoV-2 RBD specific antibodies: s309 [71] (sotrovimab), which had been proved to pan-bind with SARS-CoV-2 VOC strains.

Western blot analysis

Western blot analysis was performed as previously described procedures [72]. Briefly, cells were washed with ice-cold PBS and soluble proteins were extracted with cell lysis buffer (100mM Tris-HCl pH = 8.0, 150mM NaCl, 1% NP-40, phosphatase and protease inhibitor cocktail tablets (Abcam)) according to the manufacturer's protocol. For the analysis of S protein processing in VSV pseudotyped particles (VSVpp), we loaded 10 ml VSVpp onto 500 μl of a 20% (w/v) sucrose cushion and performed high-speed centrifugation (25000 g for 120 min at 4˚C), the concentrated particles were re-suspended in 50 μl PBS. Equal amounts of protein samples were separated by 8% sodium dodecyl sulfate-polyacrylamide gel electrophoresis (SDS-PAGE) and transferred to nitrocellulose filter (NC) membranes. Mouse monoclonal antibodies targeting FLAG tag, β-actin (TransGen Biotech, 1:5000) were used as primary antibodies, horseradish peroxidase-conjugated (HPR) goat anti-mouse IgG antibody (Southern Biotechnology Associate, 1:10000) was the second antibody. The quantitative result of the ratio of cleaved to a full-length spike in immunoblots was analyzed by Image J software.

Fusion assay

This assay utilized a split protein encoding the GFP gene, and the respective split proteins, GFP1-10 and GFP11, were expressed in effector and target cells by transfection [37]. For cell-cell fusion activity, hACE2-293T or Caco-2 cells transfected with pQCXIP-BSR-GFP11 were prepared as target cells; HEK293T expressing the wild-type (WT) or chimeric S proteins and pQCXIP-GFP1-10 were prepared as effector cells. In brief, the 293T cells were grown to 80% confluence in a 12-well plate and transfected with 1 μg pQCXIP-GFP1-10 and 1μg pcDNA3.1 (+)-SARS2 S-FLAG (WT or chimera), the hACE2-293T or Caco-2 cells in a 12-well plate were transfected with 1μg pQCXIP-BSR-GFP11. After 24h, the target cell and effector cell populations were digested with 0.25% Trypsin-EDTA solution for 1 min at room temperature, and then washed and resuspended in DMEM containing 10% FBS but no trypsin, mixed at a 4:1 ratio in different combinations, plated at 2x 10^5 cells per well in a 96-well plate, and the fluorescence images were taken at the indicated time point using a Zeiss LSM800 confocal laser scanning microscope and a Keyence all-in-one Fluorescence microscope BZ-X800. The GFP area was quantified on Image J, and the expression levels of surface S proteins were analyzed using flow cytometry, and the GFP area was normalized to the mean fluorescence intensity (MFI) of surface S proteins, and the normalized values were shown as fusion activity.

Pseudotyped particles assay

HEK293T cells were transfected with 72 μg WT or chimera S plasmid into a 15 cm cell culture dish. After 24 h, the cells were washed twice and inoculated with VSV*△G-Luc at a multiplicity of infection of 0.1 for 1h. After the inoculum was removed, the cells were washed 5 times using PBS with 2% FPS and further cultured with a DMEM culture medium for 36h. The supernatant was harvested and centrifuged at 3000 rpm to free cellular debris, filtered through a 0.45 μm syringe filter, and stored at– 80˚C in small aliquots.

To detect the neutralizing activity of antibodies, serial dilutions (1:3) of mAbs were mixed with an equal volume of 200 50% tissue culture infectious doses (TCID50) SARS2 and SARS VSVpp into a 96 well-plate and incubated for 1 h at 37˚C, and then ACE-293T cells (100 μl, 2×10^5 in DMEM) were added to all wells and incubated for further 24 h at 37˚C. Luciferase activity was analyzed by the luciferase assay system (Promega). IC50 was determined by a four-parameter logistic regression using GraphPad Prism 8.0 (GraphPad Software Inc.)

Proteins and Monoclonal antibodies expression and purification

Proteins and antibodies were generated as described previously [73]. In brief, for S proteins and ACE2, target genes were firstly amplified and subcloned to pcDNA3.1(+) vetor, and after performing Site-Directed Mutagenesis, plasmids were transfected into HEK293T cells using polyethylenimine (PEI) and cultured for 5 days. The supernatant was collected and purified using Ni-sepharose. For antibodies, the single B cells of COVID19 convalescents were obtained and then sorted into 96-well plates, and the IgG heavy and light chain variable genes were amplified by reverse transcriptase polymerase chain reaction (RT-PCR) and cloned into human IgG1 expression vectors and co-transfected into HEK293T cells with equal amounts of heavy/light-chain plasmids. Five days post-transfection, the supernatants were collected and purified using protein A agarose beads.

Rescue and infection of recombinant SARS-CoV/SARS-CoV-2 virus

2×10^6 HEK293T cells were seeded in a 6-cm plate. After recovery for 24 h, HEK293T cells were transfected with three μg Rep [41] and three μg plasmids encoding various S genes using Hieff Liposomal Transfection Reagent (Yeasen Biotech, Cat#40802ES03, Shanghai, China). Six h post-transfection, the medium containing the mixture of DNA/transfection reagent was replaced with fresh medium. After recovery for 36 to 48 h, the supernatants were collected for further use.

For the quantification of the viral particles in the supernatants, the total RNAs were extracted from the same volume of various supernatants with TRIzol LS Reagent (Thermo-Fisher Scientific, 10296010) following the manufacturer's instruction. The RNAs were subjected to quantitative RT-PCR, and the relative viral particle concentrations in various supernatants were calculated accordingly. For the further infection assay, the same amount of viral particles was used.

2×10^5 HEK293T-ACE2 cells were seeded in one well of a 6-well plate. After recovery for 24 h, the HEK293T cells were infected with recombinant SARS-CoV/SARS-CoV-2 viruses, and two h post-infection, the viruses-containing medium was replaced with fresh medium. 24 h post-infection, the cells were collected for the extraction of total RNA and/or protein.

Enzyme-linked immunosorbent assay (ELISA) to detect Spikes binding ability to ACE2

ELISA was performed as described previously [73]. High-protein binding microtiter plates (Costar) were coated with 2 μg/ml human ACE2 protein in PBS overnight at 4˚C respectively.

After 3% BSA in PBS blocking, serially diluted S proteins 1:3 starting at 50 ng/μl were incubated for 1h at 37˚C. After washing 6 times with PBST, a S2 antibody from our lab, I24, was incubated at 10 μg/ml at 37˚C for 1h, after washing again, the HPR-conjugated goat anti-human IgG antibody (Jackson Immuno Research, 1:2000) was incubated for another 1h at 37˚C. The plate was developed with Super Aquablue ELISA substrate (eBiosciences). Absorbance was measured at 405 nm on a microplate spectrophotometer (BioTek).

Effect of drug treatment on fusion ability and cell viability assay

Camostat and E64d were diluted at different concentrations first and then added to the cell mixture for fusion assay in a 96-well plate. The cell mixture was then mixed gently and cultured in a 5% CO_2 environment at 37˚C for subsequent testing.

The effects of Camostat and E64d on cell viability were measured by CCK8 assay. 293T cells were seeded into a 96-well plate and were left untreated or treated with different concentrations of drugs for 24 h. After treatments, CCK8 was added into the culture medium and incubated for 1 h at 37˚C to measure the absorbance at 405 nm.

TMPRSS2 cleavage assay

Recombinant Spike proteins were concentrated to 0.5mg/ml in Assay buffer (25mM Tris, 75mM NaCl, 2mM $CaCl_2$, PH = 8.0) and incubated with TMPRSS2, which was kindly provided by Dr. Xiong Xiaoli. Digestion took place 30 min in room temperature. After digestion, 5× loading buffer was added into the samples and boiled for 10 min at 98˚C to prepare the SDS-PAGE samples, and 2μg of Spike protein were loaded per well under each condition for subsequent western blot.

Phylogenetic analyses

We selected representative sequences from the NCBI taxonomy *Sarbecovrius* grouping and compared them using mafft software. We then used fasttree software to construct a phylogenetic tree based on SARS-like S proteins.

Statistical analysis

The Prism software (Graphpad Version 8.0) was used for all statistical analyses. The significance of differences between the two groups was determined with a two-tailed Student's t-test. One-way or two-way analysis of variances with Bonferroni correction was employed for multi-group comparison. For all analyses, only a probability (p) value of 0.05 or lower were considered statistically significant ($p > 0.05$ [ns, not significant], p % 0.05 [*], p % 0.01 [**], p % 0.001 [***]).

Supporting information

S1 Fig. Reversing IFP motif of S2-chimeric Spike influenced the fusogenicity significantly. (A and F) Schematic diagram of the S2 motif chimeric Spike. The S2 was divided into 3 parts as Fig 2 and to replace the corresponding area in turn. The F1 was further divided into two parts just as Fig 2 did. The numbers in parentheses are identical to those in Fig 3B–3E and 3F–3J. (B and G) Western blot. A representative blot of S-expressing cells (top) and quantified band intensity (the ratio of CL-S to the FL-S plus CL-S proteins) (bottom) are shown. (C and H) Flow cytometry. The summarized results of the surface S expression were shown. s309 antibody and mouse anti-human IgG-FITC were used respectively. (D and I) Spike-based fusion assay. The fusion activity was quantified by measuring the ratio of GFP+ area to DAPI area by

imaging at different times (2, 6, 12 and 24hpt). The results for SARS-CoV-2, Spike4, 15–19 or SARS-CoV, Spike2, 10–14 were shown as Saffron and grey lines, respectively. (E and J) Representative images of cell-cell fusion. Scale bar: 500 μm. Results are means +/- SD from at least three fields per condition. Results are representative of at least three independent experiments. In B and G, statistically significant differences between parental S (Spike2 or Spike4) and chimeric Spikes were determined by a two-sided paired t test (*: $p<0.05$). In D and I, statistically significant differences between parental S (Spike2 or Spike4) and chimeric Spikes were determined by Student's test at each point (*: $p<0.05$, **: $p<0.01$).
(TIF)

S2 Fig. The Influence of TMPRSS2 on Spike fusogenicity. (A) Spike-based fusion assay. The fusion activity was quantified by measuring the ratio of GFP+ area to DAPI area by imaging at different concentration of TMPRSS2 (0, 0.5, 1 and 2 μg). The results for SARS-CoV-2 and SARS-CoV were shown as Red and grey lines, respectively. (B) Representative images of cell-cell fusion. Scale bar: 500 μm. (C) Western blot. A representative blot of 293T cell lysates expressing TMPRSS2 with various concentrations. Beta-actin was used as a control. (D) Cell viability assay. The cell viability with different doses of Camostat and E64d was evaluated by CCK8 assay. Results are means +/- SD from at least three fields per condition. Results are representative of at least three independent experiments. Statistically significant differences (**: $p<0.01$) between S813 Spike and T813 Spike were determined by Student's test at each point (C, F and G).
(TIF)

S3 Fig. Spike S813T mutation of SARS-CoV-2 disturbed fusion in Non-trypsin condition. The fusion activity of Spikes with S813 or T813 were quantified in non-trypsin condition, by measuring the ratio of GFP+ area to DAPI area at different concentration: Spike expressing cells mixing with 293T cells, ACE2-293T cells or ACE2-293T/TMPRSS2 cells respectively. The results for S813 S and T813 S were shown as Red and Blue histogram, and the disturbance of fusion by S813T mutation is still observed in SARS-CoV-2, but not in SARS-CoV. After overexpressing TMPRSS2, the fusion ability increased both in SARS-CoV and SARS-CoV-2, and the influence of S813T mutation was disappeared. Representative cell-cell fusion images of SARS-CoV-2 (up) and SARS-CoV (down) were shown. Scale bar: 500 μm. Results are means +/- SD from at least three fields per condition. Results are representative of at least three independent experiments. Statistically significant differences (**: $p<0.01$) between S813 Spike and T813 Spike were determined by Student's test at each point.
(TIF)

Acknowledgments

We would like to acknowledge Dr. Wenxia Tian at College of Veterinary Medicine, Shanxi Agricultural University for providing materials, technical support and valuable suggestions. We thank Dr Hai Li at School of Basic Medical Sciences, XI'AN JIAOTONG University for suggestions and revision of the manuscript.

Author Contributions

Conceptualization: Yong Ma, Tianyi Qiu, Yao-Qing Chen.

Data curation: Yong Ma, Pengbin Li.

Formal analysis: Yong Ma, Pengbin Li, Yunqi Hu.

Funding acquisition: Yao-Qing Chen.

Investigation: Yong Ma, Pengbin Li, Yunqi Hu, Tianyi Qiu, Wenjing Zhao, Jun Chen, Xiaoli Xiong, Mang Shi, Ji-An Pan, Yao-Qing Chen.

Methodology: Yong Ma, Pengbin Li, Yunqi Hu, Tianyi Qiu, Jiaxin Zhuang, Mang Shi, Ji-An Pan.

Project administration: Yao-Qing Chen.

Resources: Hongjie Lu, Kexin Lv, Mengxin Xu, Jiaxin Zhuang, Xue Liu, Suhua He, Bing He, Shuning Liu, Lin Liu, Yuanyuan Wang, Xinyu Yue, Yanmei Zhai, Wanyu Luo, Haoting Mai, Yu Kuang, Shifeng Chen, Feng Ye, Na Zhou, Jun Chen, Shoudeng Chen.

Software: Tianyi Qiu, Mang Shi.

Supervision: Yao-Qing Chen.

Validation: Yong Ma, Pengbin Li, Yunqi Hu.

Visualization: Yong Ma, Tianyi Qiu, Lixiang Wang, Xue Liu, Mang Shi.

Writing – original draft: Yong Ma, Pengbin Li, Yunqi Hu.

Writing – review & editing: Yong Ma, Xiaoli Xiong, Mang Shi, Yao-Qing Chen.

References

1. Da Silva SJR, Do Nascimento JCF, Germano Mendes RP, Guarines KM, Targino Alves Da Silva C, Da Silva PG, et al. Two Years into the COVID-19 Pandemic: Lessons Learned. ACS Infectious Diseases. 2022; 8(9):1758–1814. https://doi.org/10.1021/acsinfecdis.2c00204 PMID: 35940589
2. Dharmarajan G, Li R, Chanda E, Dean KR, Dirzo R, Jakobsen KS, et al. The Animal Origin of Major Human Infectious Diseases: What Can Past Epidemics Teach Us About Preventing the Next Pandemic? Zoonoses. 2022; 2(1).
3. Zhou P, Yang XL, Wang XG, Hu B, Zhang L, Zhang W, et al. A pneumonia outbreak associated with a new coronavirus of probable bat origin. Nature. 2020; 579(7798):270–273. https://doi.org/10.1038/s41586-020-2012-7 PMID: 32015507
4. Cui J, Li F, Shi Z-L. Origin and evolution of pathogenic coronaviruses. Nature Reviews Microbiology. 2019; 17(3):181–192. https://doi.org/10.1038/s41579-018-0118-9 PMID: 30531947
5. Stadler K, Masignani V, Eickmann M, Becker S, Abrignani S, Klenk H-D, et al. SARS—beginning to understand a new virus. Nature Reviews Microbiology. 2003; 1(3):209–218. https://doi.org/10.1038/nrmicro775 PMID: 15035025
6. Belouzard S, Millet JK, Licitra BN, Whittaker GR. Mechanisms of Coronavirus Cell Entry Mediated by the Viral Spike Protein. Viruses. 2012; 4(6):1011–1033. https://doi.org/10.3390/v4061011 PMID: 22816037
7. Jackson CB, Farzan M, Chen B, Choe H. Mechanisms of SARS-CoV-2 entry into cells. Nature Reviews Molecular Cell Biology. 2022; 23(1):3–20. https://doi.org/10.1038/s41580-021-00418-x PMID: 34611326
8. Hoffmann M, Kleine-Weber H, Schroeder S, Krüger N, Herrler T, Erichsen S, et al. SARS-CoV-2 Cell Entry Depends on ACE2 and TMPRSS2 and Is Blocked by a Clinically Proven Protease Inhibitor. Cell. 2020; 181(2):271–280.e278. https://doi.org/10.1016/j.cell.2020.02.052 PMID: 32142651
9. Wang Q, Zhang Y, Wu L, Niu S, Song C, Zhang Z, et al. Structural and Functional Basis of SARS-CoV-2 Entry by Using Human ACE2. Cell. 2020; 181(4):894–904.e899. https://doi.org/10.1016/j.cell.2020.03.045 PMID: 32275855
10. Sun W, He L, Zhang H, Tian X, Bai Z, Sun L, et al. The self-assembled nanoparticle-based trimeric RBD mRNA vaccine elicits robust and durable protective immunity against SARS-CoV-2 in mice. Signal Transduct Target Ther. 2021; 6(1):340. https://doi.org/10.1038/s41392-021-00750-w PMID: 34504054
11. Yang S, Li Y, Dai L, Wang J, He P, Li C, et al. Safety and immunogenicity of a recombinant tandem-repeat dimeric RBD-based protein subunit vaccine (ZF2001) against COVID-19 in adults: two randomised, double-blind, placebo-controlled, phase 1 and 2 trials. Lancet Infect Dis. 2021; 21(8):1107–1119. https://doi.org/10.1016/S1473-3099(21)00127-4 PMID: 33773111

12. Zhang J, Hu Z, He J, Liao Y, Li Y, Pei R, et al. Safety and immunogenicity of a recombinant interferon-armed RBD dimer vaccine (V-01) for COVID-19 in healthy adults: a randomized, double-blind, placebo-controlled, Phase I trial. Emerg Microbes Infect. 2021; 10(1):1589–1597. https://doi.org/10.1080/22221751.2021.1951126 PMID: 34197281

13. Barnes CO, Jette CA, Abernathy ME, Dam KA, Esswein SR, Gristick HB, et al. SARS-CoV-2 neutralizing antibody structures inform therapeutic strategies. Nature. 2020; 588(7839):682–687. https://doi.org/10.1038/s41586-020-2852-1 PMID: 33045718

14. He B, Liu S, Wang Y, Xu M, Cai W, Liu J, et al. Rapid isolation and immune profiling of SARS-CoV-2 specific memory B cell in convalescent COVID-19 patients via LIBRA-seq. Signal Transduct Target Ther. 2021; 6(1):195. https://doi.org/10.1038/s41392-021-00610-7 PMID: 34001847

15. Cameroni E, Bowen JE, Rosen LE, Saliba C, Zepeda SK, Culap K, et al. Broadly neutralizing antibodies overcome SARS-CoV-2 Omicron antigenic shift. Nature. 2022; 602(7898):664–670. https://doi.org/10.1038/s41586-021-04386-2 PMID: 35016195

16. Deshpande A, Harris BD, Martinez-Sobrido L, Kobie JJ, Walter MR. Epitope Classification and RBD Binding Properties of Neutralizing Antibodies Against SARS-CoV-2 Variants of Concern. Front Immunol. 2021; 12:691715. https://doi.org/10.3389/fimmu.2021.691715 PMID: 34149735

17. Focosi D, Maggi F. Neutralising antibody escape of SARS-CoV-2 spike protein: Risk assessment for antibody-based Covid-19 therapeutics and vaccines. Rev Med Virol. 2021; 31(6):e2231. https://doi.org/10.1002/rmv.2231 PMID: 33724631

18. Greaney AJ, Starr TN, Barnes CO, Weisblum Y, Schmidt F, Caskey M, et al. Mapping mutations to the SARS-CoV-2 RBD that escape binding by different classes of antibodies. Nat Commun. 2021; 12(1):4196. https://doi.org/10.1038/s41467-021-24435-8 PMID: 34234131

19. Benton DJ, Wrobel AG, Xu P, Roustan C, Martin SR, Rosenthal PB, et al. Receptor binding and priming of the spike protein of SARS-CoV-2 for membrane fusion. Nature. 2020; 588(7837):327–330. https://doi.org/10.1038/s41586-020-2772-0 PMID: 32942285

20. Walls AC, Park YJ, Tortorici MA, Wall A, McGuire AT, Veesler D. Structure, Function, and Antigenicity of the SARS-CoV-2 Spike Glycoprotein. Cell. 2020; 181(2):281–292 e286. https://doi.org/10.1016/j.cell.2020.02.058 PMID: 32155444

21. Papa G, Mallery DL, Albecka A, Welch LG, Cattin-Ortolá J, Luptak J, et al. Furin cleavage of SARS-CoV-2 Spike promotes but is not essential for infection and cell-cell fusion. PLOS Pathogens. 2021; 17(1):e1009246. https://doi.org/10.1371/journal.ppat.1009246 PMID: 33493182

22. Tang T, Bidon M, Jaimes JA, Whittaker GR, Daniel S. Coronavirus membrane fusion mechanism offers a potential target for antiviral development. Antiviral Res. 2020; 178:104792. https://doi.org/10.1016/j.antiviral.2020.104792 PMID: 32272173

23. Yu S, Zheng X, Zhou B, Li J, Chen M, Deng R, et al. SARS-CoV-2 spike engagement of ACE2 primes S2' site cleavage and fusion initiation. Proc Natl Acad Sci U S A. 2022; 119(1). https://doi.org/10.1073/pnas.2111199119 PMID: 34930824

24. Iwata-Yoshikawa N, Okamura T, Shimizu Y, Hasegawa H, Takeda M, Nagata N. TMPRSS2 Contributes to Virus Spread and Immunopathology in the Airways of Murine Models after Coronavirus Infection. J Virol. 2019; 93(6). https://doi.org/10.1128/JVI.01815-18 PMID: 30626688

25. Zhao MM, Yang WL, Yang FY, Zhang L, Huang WJ, Hou W, et al. Cathepsin L plays a key role in SARS-CoV-2 infection in humans and humanized mice and is a promising target for new drug development. Signal Transduct Target Ther. 2021; 6(1):134. https://doi.org/10.1038/s41392-021-00558-8 PMID: 33774649

26. Xia S, Liu M, Wang C, Xu W, Lan Q, Feng S, et al. Inhibition of SARS-CoV-2 (previously 2019-nCoV) infection by a highly potent pan-coronavirus fusion inhibitor targeting its spike protein that harbors a high capacity to mediate membrane fusion. Cell Res. 2020; 30(4):343–355.

27. Basso LGM, Zeraik AE, Felizatti AP, Costa-Filho AJ. Membranotropic and biological activities of the membrane fusion peptides from SARS-CoV spike glycoprotein: The importance of the complete internal fusion peptide domain. Biochim Biophys Acta Biomembr. 2021; 1863(11):183697. https://doi.org/10.1016/j.bbamem.2021.183697 PMID: 34274319

28. Lai AL, Freed JH. Negatively charged residues in the membrane ordering activity of SARS-CoV-1 and -2 fusion peptides. Biophys J. 2022; 121(2):207–227. https://doi.org/10.1016/j.bpj.2021.12.024 PMID: 34929193

29. Santamaria A, Batchu KC, Matsarskaia O, Prévost SF, Russo D, Natali F, et al. Strikingly Different Roles of SARS-CoV-2 Fusion Peptides Uncovered by Neutron Scattering. J Am Chem Soc. 2022; 144(7):2968–2979. https://doi.org/10.1021/jacs.1c09856 PMID: 35157798

30. Coutard B, Valle C, de Lamballerie X, Canard B, Seidah NG, Decroly E. The spike glycoprotein of the new coronavirus 2019-nCoV contains a furin-like cleavage site absent in CoV of the same clade. Antiviral Res. 2020; 176:104742. https://doi.org/10.1016/j.antiviral.2020.104742 PMID: 32057769

31. Xu X, Chen P, Wang J, Feng J, Zhou H, Li X, et al. Evolution of the novel coronavirus from the ongoing Wuhan outbreak and modeling of its spike protein for risk of human transmission. Sci China Life Sci. 2020; 63(3):457–460. https://doi.org/10.1007/s11427-020-1637-5 PMID: 32009228

32. Shang J, Wan Y, Luo C, Ye G, Geng Q, Auerbach A, et al. Cell entry mechanisms of SARS-CoV-2. Proc Natl Acad Sci U S A. 2020; 117(21):11727–11734. https://doi.org/10.1073/pnas.2003138117 PMID: 32376634

33. Wrapp D, Wang N, Corbett KS, Goldsmith JA, Hsieh CL, Abiona O, et al. Cryo-EM structure of the 2019-nCoV spike in the prefusion conformation. Science. 2020; 367(6483):1260–1263. https://doi.org/10.1126/science.abb2507 PMID: 32075877

34. Madu IG, Roth SL, Belouzard S, Whittaker GR. Characterization of a highly conserved domain within the severe acute respiratory syndrome coronavirus spike protein S2 domain with characteristics of a viral fusion peptide. J Virol. 2009; 83(15):7411–21. https://doi.org/10.1128/JVI.00079-09 PMID: 19439480

35. Ou X, Zheng W, Shan Y, Mu Z, Dominguez SR, Holmes KV, et al. Identification of the Fusion Peptide-Containing Region in Betacoronavirus Spike Glycoproteins. J Virol. 2016; 90(12):5586–600. https://doi.org/10.1128/JVI.00015-16 PMID: 27030273

36. Ren W, Ju X, Gong M, Lan J, Yu Y, Long Q, et al. Characterization of SARS-CoV-2 Variants B.1.617.1 (Kappa), B.1.617.2 (Delta), and B.1.618 by Cell Entry and Immune Evasion. mBio. 2022; 13(2): e0009922. https://doi.org/10.1128/mbio.00099-22 PMID: 35266815

37. Buchrieser J, Dufloo J, Hubert M, Monel B, Planas D, Rajah MM, et al. Syncytia formation by SARS-CoV-2-infected cells. Embo j. 2020; 39(23):e106267. https://doi.org/10.15252/embj.2020106267 PMID: 33051876

38. Rajah MM, Bernier A, Buchrieser J, Schwartz O. The Mechanism and Consequences of SARS-CoV-2 Spike-Mediated Fusion and Syncytia Formation. J Mol Biol. 2022; 434(6):167280. https://doi.org/10.1016/j.jmb.2021.167280 PMID: 34606831

39. Koch J, Uckeley ZM, Doldan P, Stanifer M, Boulant S, Lozach PY. TMPRSS2 expression dictates the entry route used by SARS-CoV-2 to infect host cells. Embo j. 2021; 40(16):e107821. https://doi.org/10.15252/embj.2021107821 PMID: 34159616

40. Cocozza F, Névo N, Piovesana E, Lahaye X, Buchrieser J, Schwartz O, et al. Extracellular vesicles containing ACE2 efficiently prevent infection by SARS-CoV-2 Spike protein-containing virus. J Extracell Vesicles. 2020; 10(2):e12050. https://doi.org/10.1002/jev2.12050 PMID: 33391636

41. Jin YY, Lin H, Cao L, Wu WC, Ji Y, Du L, et al. A Convenient and Biosafe Replicon with Accessory Genes of SARS-CoV-2 and Its Potential Application in Antiviral Drug Discovery. Virol Sin. 2021; 36 (5):913–923. https://doi.org/10.1007/s12250-021-00385-9 PMID: 33999369

42. Malicoat J, Manivasagam S, Zuñiga S, Sola I, McCabe D, Rong L, et al. Development of a Single-Cycle Infectious SARS-CoV-2 Virus Replicon Particle System for Use in Biosafety Level 2 Laboratories. J Virol. 2022; 96(3). https://doi.org/10.1128/JVI.01837-21 PMID: 34851142

43. Ricardo-Lax I, Luna JM, Thao TTN, Le Pen J, Yu Y, Hoffmann HH, et al. Replication and single-cycle delivery of SARS-CoV-2 replicons. Science. 2021 Nov 26; 374(6571):1099–1106. https://doi.org/10.1126/science.abj8430 PMID: 34648371

44. Schaub JM, Chou CW, Kuo HC, Javanmardi K, Hsieh CL, Goldsmith J, et al. Expression and characterization of SARS-CoV-2 spike proteins. Nat Protoc. 2021; 16(11):5339–5356. https://doi.org/10.1038/s41596-021-00623-0 PMID: 34611365

45. Lu M, Chamblee M, Zhang Y, Ye C, Dravid P, Park JG, et al. SARS-CoV-2 prefusion spike protein stabilized by six rather than two prolines is more potent for inducing antibodies that neutralize viral variants of concern. Proc Natl Acad Sci U S A. 2022; 119(35):e2110105119. https://doi.org/10.1073/pnas.2110105119 PMID: 35994646

46. Hsieh CL, Goldsmith JA, Schaub JM, DiVenere AM, Kuo HC, Javanmardi K, et al. Structure-based design of prefusion-stabilized SARS-CoV-2 spikes. Science. 2020; 369(6510):1501–1505. https://doi.org/10.1126/science.abd0826 PMID: 32703906

47. Pallesen J, Wang N, Corbett KS, Wrapp D, Kirchdoerfer RN, Turner HL, et al. Immunogenicity and structures of a rationally designed prefusion MERS-CoV spike antigen. Proc Natl Acad Sci U S A. 2017; 114(35):E7348–e7357. https://doi.org/10.1073/pnas.1707304114 PMID: 28807998

48. Kirchdoerfer RN, Wang N, Pallesen J, Wrapp D, Turner HL, Cottrell CA, et al. Stabilized coronavirus spikes are resistant to conformational changes induced by receptor recognition or proteolysis. Sci Rep. 2018; 8(1):15701. https://doi.org/10.1038/s41598-018-34171-7 PMID: 30356097

49. Zhu Z, Chakraborti S, He Y, Roberts A, Sheahan T, Xiao X, et al. Potent cross-reactive neutralization of SARS coronavirus isolates by human monoclonal antibodies. Proc Natl Acad Sci U S A. 2007; 104 (29):12123–12128. https://doi.org/10.1073/pnas.0701000104 PMID: 17620608

50. Li F. Structure, Function, and Evolution of Coronavirus Spike Proteins. Annu Rev Virol. 2016; 3(1):237–261. https://doi.org/10.1146/annurev-virology-110615-042301 PMID: 27578435

51. Zhao MM, Zhu Y, Zhang L, Zhong G, Tai L, Liu S, et al. Novel cleavage sites identified in SARS-CoV-2 spike protein reveal mechanism for cathepsin L-facilitated viral infection and treatment strategies. Cell Discov. 2022; 8(1):53. https://doi.org/10.1038/s41421-022-00419-w PMID: 35668062

52. Ohno A, Maita N, Tabata T, Nagano H, Arita K, Ariyoshi M, et al. Crystal structure of inhibitor-bound human MSPL that can activate high pathogenic avian influenza. Life Sci Alliance. 2021; 4(6). https://doi.org/10.26508/lsa.202000849 PMID: 33820827

53. Lin JJ, Tien CF, Kuo YP, Lin EJ, Tsai WH, Chen MY, et al. Furin and TMPRSS2 Resistant Spike Induces Robust Humoral and Cellular Immunity Against SARS-CoV-2 Lethal Infection. Front Immunol. 2022; 13:872047. https://doi.org/10.3389/fimmu.2022.872047 PMID: 35585971

54. Essalmani R, Jain J, Susan-Resiga D, Andréo U, Evagelidis A, Derbali RM, et al. Distinctive Roles of Furin and TMPRSS2 in SARS-CoV-2 Infectivity. J Virol. 2022; 96(8):e0012822. https://doi.org/10.1128/jvi.00128-22 PMID: 35343766

55. Örd M, Faustova I, Loog M. The sequence at Spike S1/S2 site enables cleavage by furin and phospho-regulation in SARS-CoV2 but not in SARS-CoV1 or MERS-CoV. Sci Rep. 2020; 10(1):16944. https://doi.org/10.1038/s41598-020-74101-0 PMID: 33037310

56. Shang J, Ye G, Shi K, Wan Y, Luo C, Aihara H, et al. Structural basis of receptor recognition by SARS-CoV-2. Nature. 2020; 581(7807):221–224. https://doi.org/10.1038/s41586-020-2179-y PMID: 32225175

57. Peacock TP, Goldhill DH, Zhou J, Baillon L, Frise R, Swann OC, et al. The furin cleavage site in the SARS-CoV-2 spike protein is required for transmission in ferrets. Nat Microbiol. 2021; 6(7):899–909. https://doi.org/10.1038/s41564-021-00908-w PMID: 33907312

58. Lemmin T, Kalbermatter D, Harder D, Plattet P, Fotiadis D. Structures and dynamics of the novel S1/S2 protease cleavage site loop of the SARS-CoV-2 spike glycoprotein. J Struct Biol X. 2020; 4:100038. https://doi.org/10.1016/j.yjsbx.2020.100038 PMID: 33043289

59. Wu CT, Lidsky PV, Xiao Y, Cheng R, Lee IT, Nakayama T, et al. SARS-CoV-2 replication in airway epithelia requires motile cilia and microvillar reprogramming. Cell. 2023; 186(1):112–30.e20. https://doi.org/10.1016/j.cell.2022.11.030 PMID: 36580912

60. Ou T, Mou H, Zhang L, Ojha A, Choe H, Farzan M. Hydroxychloroquine-mediated inhibition of SARS-CoV-2 entry is attenuated by TMPRSS2. PLoS Pathog. 2021; 17(1):e1009212. https://doi.org/10.1371/journal.ppat.1009212 PMID: 33465165

61. Braun E, Sauter D. Furin-mediated protein processing in infectious diseases and cancer. Clin Transl Immunology. 2019; 8(8):e1073. https://doi.org/10.1002/cti2.1073 PMID: 31406574

62. Zhang Y, Zhang L, Wu J, Yu Y, Liu S, Li T, et al. A second functional furin site in the SARS-CoV-2 spike protein. Emerg Microbes Infect. 2022; 11(1):182–194. https://doi.org/10.1080/22221751.2021.2014284 PMID: 34856891

63. Muus C, Luecken MD, Eraslan G, Sikkema L, Waghray A, Heimberg G, et al. Single-cell meta-analysis of SARS-CoV-2 entry genes across tissues and demographics. Nat Med. 2021; 27(3):546–559. https://doi.org/10.1038/s41591-020-01227-z PMID: 33654293

64. Simmons G, Gosalia DN, Rennekamp AJ, Reeves JD, Diamond SL, Bates P. Inhibitors of cathepsin L prevent severe acute respiratory syndrome coronavirus entry. Proc Natl Acad Sci U S A. 2005; 102(33):11876–11881. https://doi.org/10.1073/pnas.0505577102 PMID: 16081529

65. Huang IC, Bosch BJ, Li F, Li W, Lee KH, Ghiran S, et al. SARS coronavirus, but not human coronavirus NL63, utilizes cathepsin L to infect ACE2-expressing cells. J Biol Chem. 2006; 281(6):3198–3203. https://doi.org/10.1074/jbc.M508381200 PMID: 16339146

66. Zhu Y, Yu D, Yan H, Chong H, He Y. Design of Potent Membrane Fusion Inhibitors against SARS-CoV-2, an Emerging Coronavirus with High Fusogenic Activity. J Virol. 2020; 94(14). https://doi.org/10.1128/JVI.00635-20 PMID: 32376627

67. Kirtipal N, Bharadwaj S, Kang SG. From SARS to SARS-CoV-2, insights on structure, pathogenicity and immunity aspects of pandemic human coronaviruses. Infect Genet Evol. 2020; 85:104502. https://doi.org/10.1016/j.meegid.2020.104502 PMID: 32798769

68. Korber B, Fischer WM, Gnanakaran S, Yoon H, Theiler J, Abfalterer W, et al. Tracking Changes in SARS-CoV-2 Spike: Evidence that D614G Increases Infectivity of the COVID-19 Virus. Cell. 2020; 182(4):812–827.e819. https://doi.org/10.1016/j.cell.2020.06.043 PMID: 32697968

69. Mansbach RA, Chakraborty S, Nguyen K, Montefiori DC, Korber B, Gnanakaran S. The SARS-CoV-2 Spike variant D614G favors an open conformational state. Sci Adv. 2021; 7(16). https://doi.org/10.1126/sciadv.abf3671 PMID: 33863729

70. Cheng YW, Chao TL, Li CL, Wang SH, Kao HC, Tsai YM, et al. D614G Substitution of SARS-CoV-2 Spike Protein Increases Syncytium Formation and Virus Titer via Enhanced Furin-Mediated Spike Cleavage. mBio. 2021; 12(4):e0058721. https://doi.org/10.1128/mBio.00587-21 PMID: 34311586

71. Pinto D, Park YJ, Beltramello M, Walls AC, Tortorici MA, Bianchi S, et al. Cross-neutralization of SARS-CoV-2 by a human monoclonal SARS-CoV antibody. Nature. 2020; 583(7815):290–295. https://doi.org/10.1038/s41586-020-2349-y PMID: 32422645

72. Ma Y, Liang Y, Wang N, Cui L, Chen Z, Wu H, et al. Avian Flavivirus Infection of Monocytes/Macrophages by Extensive Subversion of Host Antiviral Innate Immune Responses. J Virol. 2019; 93(22). https://doi.org/10.1128/JVI.00978-19 PMID: 31462573

73. Chen YQ, Wohlbold TJ, Zheng NY, Huang M, Huang Y, Neu KE, et al. Influenza Infection in Humans Induces Broadly Cross-Reactive and Protective Neuraminidase-Reactive Antibodies. Cell. 2018; 173 (2):417–429.e410. https://doi.org/10.1016/j.cell.2018.03.030 PMID: 29625056

74. Liu X, Guo L, Xu T, Lu X, Ma M, Sheng W, et al. A comprehensive evolutionary and epidemiological characterization of insertion and deletion mutations in SARS-CoV-2 genomes. Virus Evol. 2021; 7(2): veab104. https://doi.org/10.1093/ve/veab104 PMID: 35039785